# Secondary reactions of aromatics-derived oxygenated organic molecules lead to plentiful highly oxygenated organic molecules within an intraday OH exposure

Yuwei Wang[1], Chuang Li[1], Ying Zhang[1], Yueyang Li[1], Gan Yang[1], Xueyan Yang[1], Yizhen Wu[1], Lei Yao[1,2], Hefeng, Zhang[3*], Lin Wang[1,2,4,5,6] *

[1] Shanghai Key Laboratory of Atmospheric Particle Pollution and Prevention (LAP[3]), Department of Environmental Science and Engineering, Jiangwan Campus, Fudan University, Shanghai 200438, China

[2] Shanghai Institute of Pollution Control and Ecological Security, Shanghai 200092, China

[3] State Environmental Protection Key Laboratory of Vehicle Emission Control and Simulation, Vehicle Emission Control Center of Ministry of Ecology and Environment, Chinese Research Academy of Environmental Sciences, Beijing 100012, China

[4] IRDR International Center of Excellence on Risk Interconnectivity and Governance on Weather/Climate Extremes Impact and Public Health, Fudan University

[5] National Observations and Research Station for Wetland Ecosystems of the Yangtze Estuary, Shanghai, China

[6] Collaborative Innovation Center of Climate Change, Nanjing, 210023, China

** Corresponding Author: H.Z., email, zhanghf@craes.org.cn; phone, +86-10-84915586*
*L.W., email, lin_wang@fudan.edu.cn; phone, +86-21-31243568*

**ABSTRACT.** Highly oxygenated organic molecules (HOMs) can participate in new particle formation (NPF) and enhance growth of newly formed particles partially because of their low volatility. Previous studies have shown formation of HOMs via autoxidation reactions of $RO_2$ intermediates generated by OH-initiated oxidation of anthropogenic volatile organic compounds (VOCs). It was also suggested that multi-generation OH oxidation could be an important source for aromatics-derived HOMs. However, our understanding on the generation of aromatics-derived HOMs are still insufficient, especially for their formation mechanisms, which determine molar yields of HOMs and are essential to the establishment of global chemical box models related to HOMs. In this study, with a potential aerosol formation oxidation flow reactor (PAM OFR), two series of OH-initiated oxidation experiments of 1,3,5-trimethylbenzene (1,3,5-TMB) were conducted to investigate the formation of aromatics-derived HOMs. In the first series, the evolution of oxidation products of 1,3,5-TMB in an OH exposure range of $(0.5 – 5.0)\times10^{10}$ molecules cm$^{-3}$ s, equivalent to an OH exposure of 0.7 – 6.9 hours at an OH concentration ([OH]) of $2\times10^{6}$ molecules cm$^{-3}$, was investigated by a nitrate-based chemical ionization mass spectrometer and a Vocus proton-transfer-reaction mass spectrometer, indicating significant secondary OH chemistry during the ageing of stabilized first generation oxygenated products within an intraday OH exposure and formation of various HOMs with lower double bond equivalence (DBE). In addition, organonitrates, formed after the introduction of $NO_x$ into the reaction systems, further confirmed the existence of such secondary reactions. The second series of experiments was conducted with same residence time but much lower [OH], which also shows the generation of multi-generation HOMs with an [OH] as low as $1.06\times10^7$ molecules $cm^{-3}$ for 53 s, i.e., an OH exposure of around $5.86\times10^8$ molecules $cm^{-3}$ s. Our study suggests an important role of secondary OH chemistry in the oxidation of aromatics, if these oxygenated products survived long enough in the ambient, and elucidates detailed formation mechanisms of certain HOM products.

## 1 Introduction

OH radicals can react with volatile organic compounds (VOCs) in the atmosphere, converting primary pollutants to secondary ones. Generated from oxidation of VOCs, oxygenated organic molecules (OOMs) are crucial in a variety of atmospheric chemical processes, contributing efficiently to the formation of secondary organic aerosols (SOAs) and ground-level $O_3$ (Ng et al., 2010; Wang et al., 2022; Qu et al., 2021). Among the enormous number of oxygenated VOCs (OVOCs), highly oxygenated organic molecules (HOMs) have recently attracted significant attention (Bianchi et al., 2019). Most of HOMs are low volatility organic compounds (LVOCs) or extremely low volatility organic compounds (ELVOCs), and thus are able to drive the initial formation of nucleated particles under certain conditions and contribute to the subsequent growth of newly-formed particles, which finally enhance SOA formation (Tröstl et al., 2016; Lehtipalo et al., 2018; Stolzenburg et al., 2018; Mohr et al., 2019; Qiao et al., 2021).

Formation of HOMs is typically triggered by oxidation of VOCs in the gas phase. Peroxy radicals ($RO_2$) are generated at the initial step and will undergo an intramolecular hydrogen atom shift forming a hydroperoxide functionality and an alkyl radical. A molecular oxygen will rapidly attach to this alkyl radical and form a new and more oxidized $RO_2$. This reaction is called as autoxidation and the newly formed $RO_2$ can go through another autoxidation or bimolecular termination reactions to form a stabilized product (Crounse et al., 2013). Autoxidation is suggested to be responsible for widely detected HOMs in the atmosphere, because it can form highly oxygenated $RO_2$ in a short time scale. In terms of biomolecular reactions, $RO_2$ reacts appreciable only with hydroperoxyl radical ($HO_2$), NO, and another $RO_2$. The $RO_2$ reaction chain in polluted areas is largely terminated by NO, which prohibits generation of compounds with high oxidation levels and reduces yields of HOMs (Bianchi et al., 2019).

Nevertheless, autoxidation reactions alone are not enough to explain the large numbers of oxygen atoms and low double bond equivalence (DBE, calculated as $nC - \frac{nH+nN}{2} + 1$ where $nC, nH,$ and nN stand for number of containing carbon, hydrogen, and nitrogen, respectively) in HOMs observed in laboratory experiments and ambient campaigns. Take alkylbenzenes as an example, previous studies suggest that the main products of OH-initiated oxidation of alkylbenzenes ($C_xH_{2x-6}$, x=7, 8, or 9), i.e., bicyclic peroxy radicals (BPR, $C_xH_{2x-5}O_5\cdot$, x=7, 8, or 9) (Jenkin et al., 2003), can undergo an autoxidation reaction and form a new peroxy radical, $C_xH_{2x-5}O_7\cdot$ (x=7, 8, or 9) (Wang et al., 2017).The autoxidation of BPR could be fast if it has a favorable structure, as found in a previous study  (Wang et al., 2017). On the other hand, the structure of resulting $C_xH_{2x-5}O_7\cdot$ is strongly different from that of BPR, whose autoxidation reaction rate can be as low as the order of 0.001 $s^{-1}$, since it lacks enhancements from favorable transition state geometries and substitutes or resonance structures (Bianchi et al., 2019; Otkjær et al., 2018). Such a slow autoxidation reaction rate cannot explain the extensive existence of HOM monomers with more than 7 oxygen atoms and HOM dimers with more than 10 oxygen atoms, which are the maximum numbers of oxygen atoms in stabilized monomer and dimer products, respectively, formed from $C_xH_{2x-5}O_7\cdot$ (Molteni et al., 2018; Wang et al., 2020b; Mentel et al., 2015). Another possibility is the formation of a second oxygen bridge after the hydrogen shift of BPR (Molteni et al., 2018), but this reaction pathway would not allow a further oxygenation reaction without a breakage of the carbon ring, which is also unpromising. A very recent investigation offers new insights into the formation mechanism of these products, indicating the molecular rearrangement of BPR can initiate a series of autoxidation (Iyer et al., 2023). However, the formation mechanism of HOMs with a large hydrogen atom number, i.e., low DBE, is still vague. For example, monomer products with 16 hydrogen atoms in the OH-initiated oxidation of TMB and with 14 hydrogen atoms in the OH-initiated oxidation of xylene were observed in the laboratory, both with a DBE of 2 lower than their precursors' (Molteni et al., 2018), but their formation mechanisms cannot be explained by any known mechanisms with only one OH attack.

Multigeneration reactions of VOCs complicate HOMs' formation. Previous studies indicate that HOMs can also be formed by sequential oxidation of stabilized first-generation products of benzene and toluene (Garmash et al., 2020; Cheng et al., 2021). Garmash et al. (2020) conducted OH oxidation experiments of benzene and toluene with an OH exposure equivalent to atmospheric oxidation times of 10 hours – 15 days at OH concentrations of ~$10^6$ molecules $cm^{-3}$. Cheng et al. (2021) simulated oxidation of benzene and toluene with an OH exposure equivalent to 2.4 – 19.4 days of atmospheric photochemical ageing. Certainly, such extremely high OH exposures favor secondary OH chemistry and help to facilitate our understanding on product distributions, but such a long timescale limits atmospheric implications of their results, given the complex physical and chemical processes at night.

Compared to benzene and toluene, trimethylbenzene (TMB) is a precursor characterized with much larger HOM molar yields when reacted with OH, and the abundance of TMB in the atmosphere is unignorable (Molteni et al., 2018; Yuan et al., 2012). Previous laboratory experiments on TMB-derived HOMs mainly focused on the autoxidation reactions of BPR and the influences of $NO_x$, while the quantity of experiments was finite, restricting the application of their conclusions to the more atmospheric relevant condition (Tsiligiannis et al., 2019; Wang et al., 2020b). From the mechanism perspective, a number of HOM monomers with more than 7 oxygen atoms detected in the OH-initiated oxidation of TMB were previously assumed to be generated via multiple autoxidation reactions (Molteni et al., 2018). Nevertheless, a subsequent OH oxidation of the first-generation oxygenated products might be more plausible for the formation of HOM monomers with more than 7 oxygen atoms from the present point of view. Indeed, laboratory experiments show that $RO_2$ formed during the second-generation OH oxidation of the first-generation stabilized oxidation products can also undergo autoxidation reactions, which entangles reaction mechanisms potentially involved in the formation of those HOMs and justifies more investigations on the multigeneration OH oxidation of aromatics (Wang et al., 2020b). OH with an atmospheric concentration ([OH]) up to $6\times10^6$ – $2.6\times10^7$ molecule $cm^{-3}$, which is several times higher than the typical average atmospheric [OH], $1.5\times10^6$ molecule $cm^{-3}$ (Jacob, 1999), has been frequently observed in both urban and suburban environments in China (Tan et al., 2019; Lu et al., 2012), leading to a realistic implication of multigeneration OH oxidation. Therefore, it is imperative to study chemical characteristics of formation reactions of HOMs at different OH exposures, especially those fewer than or equivalent to one day of atmospheric oxidation.

In this study, a series of laboratory experiments were conducted on the OH-initiated oxidation of 1,3,5-TMB, selected as an example of anthropogenic VOCs with [OH] as high as $9.32\times10^7$ – $1.03\times10^9$ molecule $cm^{-3}$ and an OH exposure equivalent to atmospheric oxidation times of roughly 0.7 – 6.9 hours at an average daytime [OH] of $2.0\times10^6$ molecules $cm^{-3}$. A nitrate-based chemical ionization mass spectrometer (nitrate CIMS) and a Vocus proton-transfer-reaction mass spectrometer (Vocus PTR) were deployed to measure the oxidation products and the precursor, respectively. From the evolution of oxygenated products, we explored secondary OH chemistry of stabilized first-generation oxygenated products generated by the oxidation of 1,3,5-TMB. Furthermore, the influence of NO on the formation of HOMs was investigated by introducing $N_2O$ into the reaction system via formation of organonitrates. In addition, another series of experiments under atmospheric relevant [OH] were conducted to confirm the applicability of the above-developed multi-generation OH oxidation mechanisms in the ambient atmosphere.

## 2 Methods

OH-initiated oxidation of 1,3,5-TMB was investigated in a potential aerosol formation oxidation flow reactor (PAM OFR) system at $T = 298 \pm 1$ K and a pressure of 1 atm (Lambe et al., 2015). Two series of experiments were conducted, one under high [OH] conditions and the other under low [OH] conditions. Hereafter, we refer to the series of high [OH] experiments as 'the 1st-round experiments' and the low [OH] as 'the 2nd-round experiments', respectively. The $i^{th}$ experiment in the 1st-round experiments is labelled as 1-*i* and the one in the 2nd-round experiments as 2-*i*, where *i* stands for its serial number. The experimental settings in this study differed slightly from what were used previously (Wang et al., 2020b). In the 1st-round experiments, forty OH experiments without $NO_x$ (Exp. 1-1 – 1-40) and twenty-eight experiments with $NO_x$ (Exp. 1-41 – 1-68) were performed. Seven experiments were conducted in the 2nd-round, four without $NO_x$ and three with $NO_x$. The experimental conditions are summarized in Table S1, including concentrations of the precursor, ozone, and NO and $NO_2$. The equivalent OH exposure in the OFR for each experiment was estimated according to the precursor consumption, also listed in Table S1. OH exposures in the OFR were in the range of $(5.2 - 48.7) \times 10^9$ and $(0.6 - 5.5) \times 10^9$ molecules $cm^{-3}$ s in the 1st-round and 2nd-round experiments, respectively.

A home-made 1,3,5-TMB/$N_2$ cylinder was used as a stable gaseous precursor source in the experiments, from which the flow rate of 1,3,5-TMB/$N_2$ varied between 1 – 3 sccm (standard cubic centimeter per minute, standard to 0 °C, 1 atm), leading to 28.9 – 62.7 ppb of 1,3,5-TMB in the 1st-round experiments, and 30.8 or 34.5 ppb of 1,3,5-TMB in the 2nd-round experiments, respectively (Table S1). A total flow of 15 slpm (standard liters per minute, standard to 0 °C, 1 atm) zero-gas generated by a zero-gas generator (model 737-13, Aadco Instruments Inc.), together with the 1,3,5-TMB/$N_2$ flow, was introduced into the OFR. The reaction time in both series of experiments was kept at around 53 s and the flow reactor was kept as a plug flow in both series. The flow in the PAM OFR is laminar with a very low axial mixing, as characterized with a Taylor dispersion model in a previous study (Lambe et al., 2011). Among the 15 slpm zero-gas, 6 slpm was initially passed through a Nafion humidifier (Perma Pure Model FC100-80-6MSS) filled with ultra-pure water and finally converged with the main flow into the OFR to achieve and keep a desired RH of 20.0 ± 2.5 % in the OFR throughout all the experiments, and 2 slpm was initially passed through a separate ozone chamber, resulting in an initial ozone concentration of around 429 – 881 ppb in the OFR in the 1st-round experiments and 123 – 152 ppb in the 2nd-round experiments, respectively. The OFR was operated with only the 254 nm lights on, under which the primary oxidant production reactions in the OFR were $O_3 + hv\ (254\ nm) \rightarrow O_2 + O(^1D)$ and $O(^1D) + H_2O \rightarrow 2OH.$ After turning on of UV lights, a certain HOM compound is believed to be generated if its signal is more than 3 standard deviations of its background signal. If the fluctuations in the 1-min-averaged signals of both TMB in the Vocus PTR and typical HOMs (i.e., $C_9H_{14}O_7(NO_3)^-$) in the nitrate CIMS are within 2% during a 10-min period, we assume that a steady state has been reached. It usually took around no more than 2 minutes for the signals of HOMs to stabilize after the adjustment of UV lights. We typically monitored the reaction products for around 20 minutes for each experiment. An ozone monitor (Model 106-M, 2B technologies) and a trace-gas analyzer for NO-$NO_2$-$NO_x$ (Thermo, 42i-TL) were placed at the exit of the OFR to measure concentrations of ozone and $NO_x$, respectively.

Non-tropospheric VOC and OVOC photolysis is a typical issue that should be taken into account when evaluating the settings of OFR laboratory experiments, especially under the high UV light dose settings in the 1st-round experiments. Photolysis of the precursor and HOMs were evaluated, showing that photolysis was not a contributor to our observation. The photolysis rate of 1,3,5-TMB can be estimated based on the absorption cross-sections of 1,3,5-TMB at 254 nm (Keller-Rudek et al., 2013) and UV photon fluxes estimated by a chemistry model discussed in the following sections. The ratio of photolysis-to-OH reaction in our 1st-round experiments was merely 0.010 – 0.033. Hence, photolysis of 1,3,5-TMB was insignificant in the OFR. For stabilized products such as C9 and C18 HOMs, the cross sections of organic molecules are usually ~ $3.9\times10^{-18}$ - $3.9\times10^{-17}$ $cm^2$ (Peng et al., 2016), while the reaction rate between OH and the stabilized first-generation products are estimated to be around $1.28\times10^{-10}$ $molecule^{-1}\ cm^3\ s^{-1}$, as suggested by MCM (Jenkin et al., 2003). Hence, the ratio of photolysis rates of C9 and C18 HOMs to their secondary OH oxidation rates is estimated to be merely around 0.020 – 0.056 in the 1st-round experiments. In the 2nd-round, the influences of photolysis should be even lower due to the much lower light intensity.

For experiments with $NO_x$ in the 1st-round experiments, 350 sccm $N_2O$ (99.999%, Air Liquid) was added into the OFR to produce and sustain $NO_x$ mixing ratios at levels that were sufficiently high to be a competitive sink for $RO_2$ radicals. NO and $NO_2$ were produced via the reaction $N_2O + O(^1D) \rightarrow 2NO,$ followed by the reaction $NO + O_3 \rightarrow NO_2 + O_2.$ Two sets of irradiance intensities were chosen for $NO_x$ experiments, generally resulting in two $NO_x$ levels, 1.8 ppb NO + 70 ppb $NO_2$ (Exp. 1-41 – 1-54) and 4.8 ppb NO + 120 ppb $NO_2$ (Exp. 1-55 – 1-68) at the exit of the OFR. With the aim to slightly modify OH exposure but keep $NO_x$ concentrations constant among each set of experiments, the initial concentrations of 1,3,5-TMB were adjusted in a large range (16.7 – 84.1 ppb), as an increase in the precursor concentration corresponds to a larger sink for OH, while RH and irradiances were not changed. In the 2nd-round experiments, due to the lower ($O^1D$) in the PAM OFR, 2.5 slpm pure $N_2O$ was utilized instead, whereas the total flow rate was kept the same as that in the 1st-round. We lowered the light intensity to obtain lower [OH] in the PAM OFR, which also resulted in fluctuations in the NO concentrations ([NO]) from 1.3 to 7.1 ppb and the $NO_2$ concentrations ([$NO_2$]) from 11 to 38 ppb.

A nitrate CIMS (Ehn et al., 2014; Eisele and Tanner, 1993) and a Vocus PTR (Krechmer et al., 2018) were deployed at the exit of the OFR to measure the oxidation products of 1,3,5-TMB in the 1st-round experiments. These two mass spectrometers have been well characterized in a previous study (Wang et al., 2020b).

The sample flow rate for the nitrate CIMS in the 1st round-experiments was 8 slpm through a Teflon tube with an outer diameter (OD) of 1/4 in. and a length of 70 cm. The sheath flow for the nitrate CIMS was supplied by a zero-gas generator at a flow rate of 15 slpm. Mass resolution was approximately 8000 for ions with m/z larger than 200 Th. HOMs generated from TMB oxidation were charged in the ambient pressure interface region by collisions with nitrate clusters, $(HNO_3)_x{\cdot}NO_3^-$ ($x = 0 – 2$), and detected by nitrate CIMS as clusters with $NO_3^-$, i.e., $HOM{\cdot}NO_3^-$ (Hyttinen et al., 2015). In addition, HOMs' signals were corrected with relative transmission efficiencies of our nitrate CIMS obtained via a method reported previously (Heinritzi et al., 2016). We followed the same sampling method of PAM OFR as those in previous studies, in order to obtain a similar flow tube residence time distributions (RTDs) and thus validate usage of a modified PAM_chem_v8 model to estimate concentrations of radicals in the OFR as discussed below. We acknowledge that this is not a perfect sampling setting for nitrate CIMS. However, the reduction in the sampling efficiencies of various HOMs is likely to be close, if not identical, which keeps the distributions of HOMs.

Vocus PTR was applied to quantify precursor concentrations and measure volatile and intermediate volatility oxidation products. The focusing ion-molecule reactor (FIMR) was heated up and its temperature was maintained at 100 °C during the experiments. The FIMR can be operated under 2.0 mbar without a strong interference from corresponding water clusters when ionizing the neutral compounds. The Vocus front and back voltages were 650 V and 15 V, respectively, forming an axial voltage of 635V and a reduced electrical field (*E/N*, where E is the electric field strength and N is the number density of the buffer gas in FIMR) of 180 Td. The radio frequency (RF) voltages and frequency were set to be 450 V and 1.3 MHz, respectively. The sample flow was introduced to the Vocus PTR through a Teflon tube with an OD of 1/4 in. and a length of 120 cm from the OFR. A total sample flow of 1.4 slpm was maintained by a pump with an orifice to minimize the delay time of sampling, from which approximately 125 sccm was sampled into the FIMR through a capillary tube.

In the 2nd-round experiments, , a Vocus CI-TOF (Towerk AG, Switzerland) equipped with a Vocus Aim inlet and the same nitrate-ion chemical ionization source as adopted in the 1st-round experiments was utilized to measure oxidation products, hereafter referred as nitrate CI-TOF. The nitrate CI-TOF was characterized with a flat transmission efficiency between m/z 60 Th and m/z 500 Th, as well as a mass resolution of 10000 at m/z 200 Th. In this series of experiments, the reaction products were sampled from the PAM OFR via a 30 cm-long Teflon tube with a 1/2 in. OD to our nitrate CI-TOF. The Vocus PTR and the ozone monitor were connected to the PAM OFR from a separate port via a 120 cm-long Teflon tube with a 1/4 in. OD.

We did not quantify HOMs' concentrations. Since the inner diameters of PAM OFR, sampling tube, and the nitrate CIMS inlet were different, and two reducing unions were used during sampling, the estimation of the penetration efficiency and sampling efficiency of HOMs are of a significant uncertainty. The initial concentrations of TMB utilized in both sets of experiments fluctuated slightly, which resulted from sample preparation processes and were more obvious in the 1st-round experiments. Therefore, in the discussion on the data of the 1st-round experiments, we tried to minimize potential influences of the differences in the initial TMB concentrations on the signals of HOMs by normalizing the HOMs signals with the initial TMB signal. To precisely illustrate changes in the abundance of HOMs at different OH exposures, a normalized signal was chosen to present the abundance of detected HOMs, which is defined as the ratio of the signals of HOMs in the nitrate CIMS normalized by the reagent ions and the initial signal of 1,3,5-TMB, i.e., $S(HOMs)/S(TMB)$. $S(HOMs)$ is the signal of HOM detected by the nitrate CIMS normalized with the signal of reagent ions, whereas $S(TMB)$ is the initial signal of 1,3,5-TMB detected by the Vocus PTR.

To compare chemical regimes of the two series of experiments and the ambient atmosphere, a PAM chemistry model (PAM_chem_v8), utilized widely in previous studies, were chosen with the latest updates to calculate radical profiles in our OFR (Li et al., 2015; Cheng et al., 2021; Wang et al., 2020b; Mehra et al., 2020; Lambe et al., 2015, 2018; Peng and Jimenez, 2020; Lambe et al., 2017). This model is based on a photochemical box model that includes chemistry of photolysis of oxygen, water vapor, and other trace gases by the primary wavelengths of mercury lamps, and simplified VOC and $RO_2$ chemistry (Table S2), but further reactions of the first-generation stabilized products and the second-generation organic radicals are not considered. The detailed reactions involved with $RO_2$ include:

$$RO_2 + R'O_2 \rightarrow RO + R'O + O_2 \qquad (R1)$$

$$RO_2 + R'O_2 \rightarrow R = O + R'OH + O_2 \qquad (R2)$$

$$RO_2 + R'O_2 \rightarrow ROH + R' = O + O_2 \qquad (R3)$$

$$RO_2 + R'O_2 \rightarrow ROOR' + O_2 \qquad (R4)$$

$$RO_2 + HO_2 \rightarrow ROOH + O_2 \qquad (R5)$$

$$RO_2 + OH \rightarrow Products \qquad (R6)$$

$$RO_2 \xrightarrow{isomerization} Products \qquad (R7)$$

$$RO_2 + NO \rightarrow RO + NO_2 \qquad (R8)$$

$$RO_2 + NO \rightarrow RONO_2 \qquad (R9)$$

$$RO_2 \rightarrow physical\ loss \qquad (R10)$$

$R1$, $R2$, and $R3$ are reactions of $RO_2$ + $RO_2$, forming alkoxy radicals, carbonyl termination products, and hydroxyl termination products, respectively. $R4$ is the accretion reaction, forming dimers via combination of two monomeric $RO_2$. $R5$ is the reaction between $RO_2$ and $HO_2$, forming hydroperoxyl radicals. $R6$ is the reaction between OH and $RO_2$, whose reaction channels/products are proposed according to previous studies (Table S3). $R7$ is the unimolecular reactions of $RO_2$ in the PAM OFR, among which the autoxidation reaction rate is the most significant. $R8$ and $R9$ are the reactions between NO and $RO_2$, generating alkoxy radicals and organonitrates, respectively. $R10$ is the physical loss of $RO_2$.

Kinetic data in the modified PAM_chem_v8 are obtained from the IUPAC (International Union of Pure and Applied Chemistry) dataset (https://iupac-aeris.ipsl.fr, last access: 26 October 2023) and the MCM dataset (MCM v3.3.1, https://mcm.york.ac.uk/MCM/, last access: 9 October 2023), except for those that are specifically discussed in details in the supplement. Note that the total $RO_2$ concentration is simplified to be the sum of concentrations of BPR and $C_9H_{13}O_7\cdot$. In this work, the autoxidation reaction and the accretion reaction of 1,3,5-TMB-derived BPR, as well as the subsequent reactions of the autoxidation product of BPR, i.e., $C_9H_{13}O_7\cdot$, are newly implemented or modified in this model (Reaction No. 46 – 62 in Table S2). The newly implemented or modified reactions in this model are discussed in Supplementary Text S1. $NO_x$-related reactions are also included in the model. When we simulate experiments without $NO_x$, these reactions do not contribute to the simulation results.

For the 1st-round experiments, the input parameters of temperature, mean residence time, water vapor concentration, $O_3$ concentration, and the initial 1,3,5-TMB concentration are 25 °C, 53 s, 0.63%, 500 ppbv, and 50 ppbv, respectively, as measured directly. For the 2nd-round experiments, the input parameters of $O_3$ concentration and the initial 1,3,5-TMB concentration were updated as 150 ppbv and 30.8 ppbv, respectively. In the $NO_x$ experiments, the input flow rate of $N_2O$ is 350 sccm in the 1st-round experiments and 2.5 slpm in the 2nd-round experiments, respectively. The actinic flux at 254 nm, $I_{254}$, is constrained by comparing OH exposures by model output and OH exposures estimated by the consumption of 1,3,5-TMB as measured by a Vocus PTR. Consumption of $O_3$ estimated by the model agrees well with the measured results, with discrepancies being always within 10% at different OH exposures.

## 3 Results and discussion

### 3.1 Comparison of chemical regimes

Concentration profiles of OH, $RO_2$, and $HO_2$ as a function of OH exposures in our high [OH] experiments without $NO_x$, i.e., the 1st-round experiments, are illustrated in Figure S1a. According to the modified PAM_chem_v8, when [OH] increased from $9.32\times10^7$ to $1.03\times10^9$ molecule $cm^{-3}$, [$HO_2$] increased from $7.25\times10^8$ to $2.79\times10^9$ molecule $cm^{-3}$, whereas [$RO_2$] concentrations increased from $5.17\times10^9$ to $9.5\times10^9$ molecule $cm^{-3}$. The radical concentrations in high [OH] experiments with $NO_x$ (Figure S1b) varied in a similar range, with [$RO_2$] ranging from $4.38\times10^9$ to $9.13\times10^9$ molecule $cm^{-3}$, $HO_2$ ranging from $4.47\times10^9$ to $6.47\times10^9$ molecule $cm^{-3}$, and OH ranging from $3.86\times10^8$ to $7.82\times10^8$ molecule $cm^{-3}$, respectively. The ratios between $HO_2$/OH and $RO_2$/OH in the 1st-round experiments were generally in the same order of magnitude with the ambient atmosphere (Whalley et al., 2021).

Radical concentrations were also estimated by the PAM_chem_v8 model to illustrate the chemical regimes in the 2nd-round experiments (Table S4). The average [$HO_2$], [OH], and [$RO_2$] were $9.7\times10^7$, $1.64\times10^7$, and $1.69\times10^9$ molecule $cm^{-3}$, respectively, in Exp. 2-3, and were $6.7\times10^7$, $1.04\times10^7$, and $1.34\times10^9$ molecule $cm^{-3}$, respectively, in Exp. 2-4, both of which generally differ by no more than a factor of 3 from the summer daytime ambient ones in polluted atmosphere (Tan et al., 2017, 2018, 2019; Whalley et al., 2021; Lu et al., 2012). The average [$HO_2$], [OH], and [$RO_2$], as well as the NO and $NO_2$ concentrations in Exp. 2-7 are generally very close to those in the same environment (Tan et al., 2019).

**(a)**

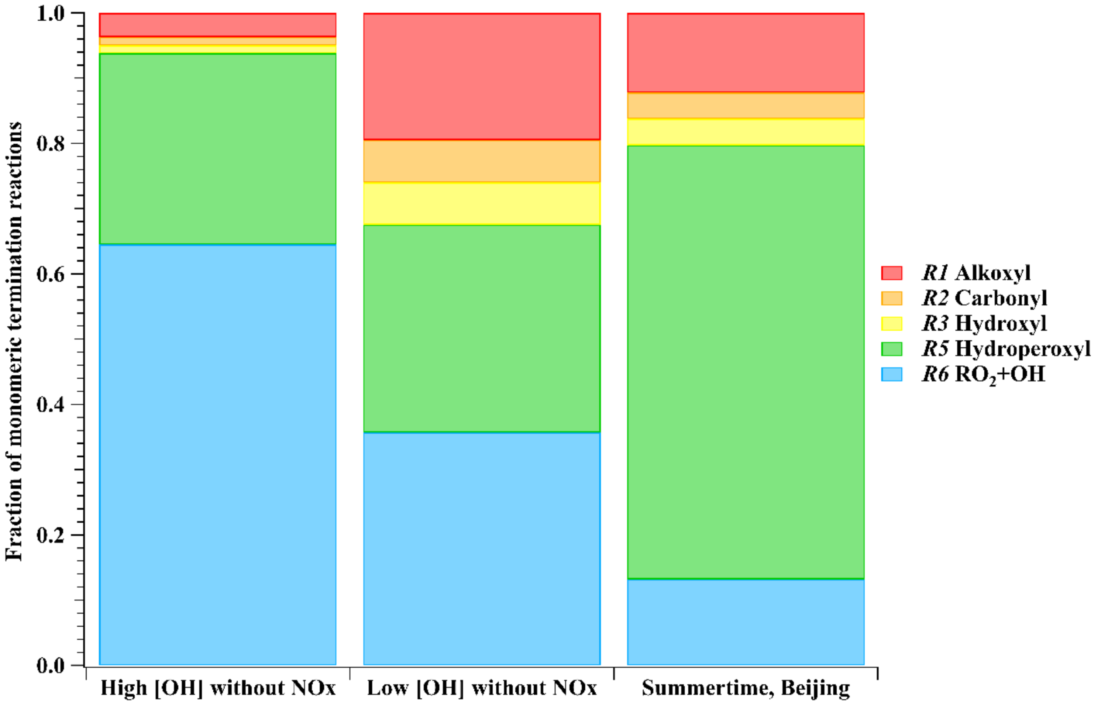

339

340 **(b)**

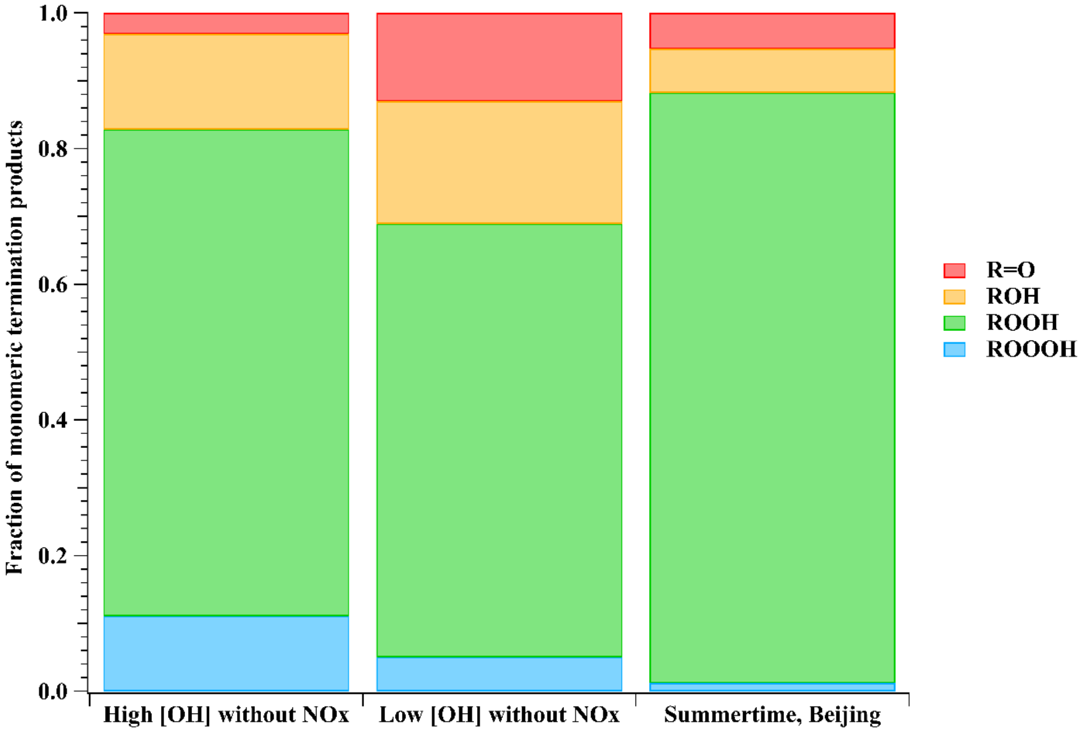

341

342 **(c)**

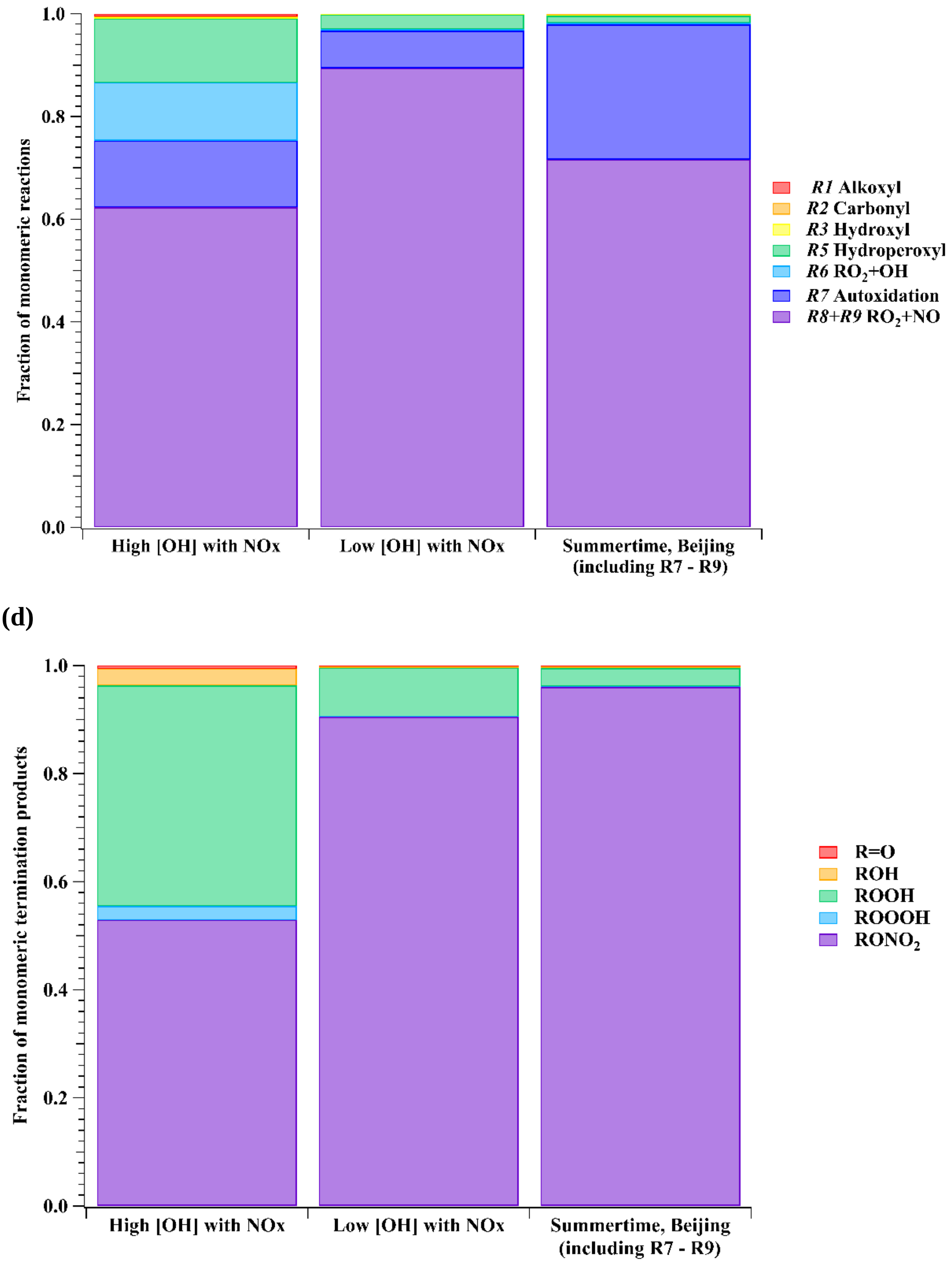

**Figure 1.** (a) The fraction of monomeric termination reactions and (b) monomeric termination products of BPR in a representative high [OH] experiment without $NO_x$ (Exp. 1-12), a representative low [OH] experiment without $NO_x$ (Exp. 2-3), and summertime, urban Beijing (Whalley et al. 2021). $NO_x$ related reactions and products for the Beijing study are not included for a better comparison. (c) The fraction of monomeric reactions (R1 - R3 and R5 - R9) and (d) monomeric termination products of BPR in a representative high [OH] experiment with $NO_x$ (Exp. 1-48), a representative low [OH] experiment with $NO_x$ (Exp. 2-7), and summertime,

urban Beijing (Whalley et al. 2021). Reactions and kinetic rate coefficients used in the calculations are provided in Table S2.

We take Exp. 1-12 ([OH] = ~$8.47\times10^8$ molecule $cm^{-3}$ and $NO_x$ = 0) and Exp. 2-3 ([OH] = ~$1.64\times10^7$ molecule $cm^{-3}$ and $NO_x$ = 0) as representative examples and compare simulation results with those from the ambient atmosphere, since $NO_x$ in the ambient is believed not to impact relative ratios for $R1 – R3$, $R5$, and $R6$. In the ambient atmosphere, the average [$HO_2$], [OH], and [$RO_2$] were $2.7\times10^8$, $8.0\times10^6$, and $1.4\times10^9$ molecule $cm^{-3}$, respectively, around summertime noon in urban Beijing (Whalley et al. 2021), and (4 - 28)$\times10^8$, (0.8 - 2.4)$\times10^7$, and $1.2\times10^9$ molecule $cm^{-3}$ (modeled) at a suburban site in Yangtze River Delta (Ma et al. 2022). As shown in Figure 1a, for the most important $RO_2$, BPR, the fractions of monomeric termination reactions of $RO_2$ + $RO_2$ ($R1 – R3$), $RO_2$ + $HO_2$ ($R5$), and $RO_2$ + OH ($R6$) were 6.2%, 29.3%, and 64.5%, respectively, in Exp.1-12. In contrast, the fractions were 32.5%, 31.8%, and 35.7%, respectively, in Exp. 2-3, whereas the values were 20.3%, 66.6%, and 13.2%, respectively, for summertime, urban Beijing.

Our $NO_x$-free experiments are characterized with an inherent drawback that the proportion of the $HO_2$ termination pathway ($R5$) is actually lower than that under ambient conditions, which is similar to most other laboratory experiments (Bianchi et al., 2019). In our high [OH] experiments without $NO_x$, the reaction rates of unimolecular reactions e.g., autoxidation reaction ($R7$) and condensation ($R10$) did not change with [OH] that increased in our experiments relative to that in the ambient. As a result, relative proportions of autoxidation and condensation are lowered. On the other hand, 1,3,5-TMB-derived BPR was suggested to undergo autoxidation ($R7$) at a reaction rate of 0.078 $s^{-1}$ (Wang et al., 2017), which represents 36.8%, 94.4%, and 92.8% of the overall rates of $R1$ - $R3$ and $R5$ - $R7$ in Exp. 1-12, Exp. 2-3, and summertime, urban Beijing, respectively. Because of its dominant proportion in Exp. 2-3 and the ambient, the autoxidation channel is not included for clarity in Figure 1a. Autoxidation does possess a lower significance in our high [OH] experiments due to the other accelerated bimolecular reactions. However, it would only influence the oxygen content of our products but would not change the DBE. Both accretion reaction ($R4$) and condensation ($R10$) have been taken into account in the model, but they would not influence the distributions of monomeric stabilized products. We will specifically discuss these two pathways in the following sections because of their complexity between the laboratory and ambient conditions.

$RO_2$ other than BPR and $C_9H_{13}O_7\cdot$ existed in the PAM OFR, which were not included in the model simulation. Their reaction rates of the accretion reaction ($R4$) and the autoxidation reaction ($R7$) should be different from BPR and $C_9H_{13}O_7\cdot$ due to the strong dependence of these two reaction rates on the molecular structure. Rates for the other channels, on the other hand, should be the same as those of BPR and $C_9H_{13}O_7\cdot$. Therefore, their fates in terms of the monomeric termination reactions ($R1$ - $R3$, $R5$ - $R6$, and $R8$ - $R9$) should be similar as BPR and $C_9H_{13}O_7\cdot$.

Calculated from yields of stabilized monomeric termination products of BPR, the fractions of monomeric termination reaction products in Exp. 1-12, Exp. 2-3, and summertime, urban Beijing (Whalley et al. 2021) are presented in Figure 1b, showing a lot of similarities between these conditions. The fractions of R=O, ROH, ROOH, and ROOOH in Exp. 1-12 were 3.1%, 14.1%, 71.7%, and 11.1%, respectively. These fractions were 13.0%, 18.1%, 63.9%, and 5.0%, respectively, in the Exp. 2-3, whereas the values were 5.3%, 6.5%, 87.0%, and 1.2%, respectively, in the summertime Beijing case. Among them, the majority of products are always ROOH and ROH, with ROOH being the most abundant. Therefore, the monomeric termination products of BPR in our experiments are atmospheric relevant. In addition, only the R=O product has a DBE higher than the reacted $RO_2$, but merely accounted for a limited proportion. All the other stabilized termination products have a DBE that is 1 lower than the precursor, and are the majority in both laboratory and ambient conditions. This indicates that the majority of the first-generation products typically have a DBE that is 1 lower than that of 1,3,5-TMB, whereas the majority of subsequent-generation products typically have a DBE that is 2 lower than that of 1,3,5-TMB. Once a monomeric compound with a DBE that is ≥2 lower than that of 1,3,5-TMB was observed, multi-generation OH reactions have happened in the system.

In experiments in absence of $NO_x$ (e.g., Exp.1-12), the proportions of $R8$ - $R9$ , i.e., the NO channel in the urban atmosphere were attributed to termination reactions of $R1$ - $R6$, i.e., $RO_2 + RO_2$, accretion reaction, $RO_2 + HO_2$, and $RO_2 + OH$. By expanding proportions of these termination reactions, laboratory investigations on product distributions can be facilitated, as the detection of certain HOM products became more precise and the mass spectra became simplified.

In experiments with $NO_x$, the chemical fates of BPR in high [OH] experiments (Exp. 1-48 as an example, [OH] = ~$6.77\times10^8$ molecule $cm^{-3}$, NO = ~1.93 ppb. $NO_2$ = ~68 ppb), low [OH] experiments (Exp. 2-7 as an example, [OH] = ~$1.69\times10^7$ molecule $cm^{-3}$, NO = ~1.30 ppb. $NO_2$ = ~11 ppb), and the summertime, urban Beijing are compared. As shown in Figure 1c, in all three conditions, $RO_2$ reactions with NO were always the most significant pathway, with autoxidation being the second most significant.

Accounting for at least 52% of monomeric termination products under all conditions, organonitrates were always the most important termination products, as shown in Figure 1d. On the other hand, based on the formulae of organonitrates, the detailed formulae for monomer $RO_2$ could be probed, which can help us better understand the chemical reactions inside the system. Alkoxy radicals generated in the NO termination channel will unlikely influence the distributions of C9 stabilized products since they tend to get decomposed in the subsequent reactions, as discussed in the Supplementary Text S1.

Due to the complexity of ambient $RO_2$ pool, it is difficult to estimate the detailed fraction of accretion reactions $R4$. In the laboratory experiments, $RO_2$ pool mainly consists of BPR and its autoxidation reaction product $C_9H_{13}O_7\cdot$, which both can undergo accretion reaction rapidly (Berndt et al., 2018b). The concentrations of these two radicals were estimated by PAM_chem_v8 according to the kinetics discussed in Supplementary Text S1. The reaction rate of accretion ($R4$) for BPR was around 1.61 $s^{-1}$ in Exp.1-12, being 61.8% of $R1 - R7$, and was 0.29 $s^{-1}$ in Exp.2-3, equivalent to 21.1% of $R1 - R7$. Certain uncertainties exist in the estimation of the proportions of accretion reactions, as the PAM_chem_v8 model only includes the first-generation reactions of precursors, whereas the subsequential fragmentation and re-initiation of stabilized products can generate a series of new $RO_2$ that will influence the proportions of accretion reactions. We are only certain that the significance of accretion reactions in both Exp. 1-12 and Exp. 2-3 is larger than the ambient. The much-expanded proportion of HOM dimers through accretion reactions makes it inadequate to compare yields of HOM dimers and HOM monomers. However, this deviation will not influence our conclusion on multi-generation OH oxidation and identification of HOM dimers can help us identify the exact $RO_2$ in the OFR and confirm the conditions of secondary OH oxidation according to the number of hydrogen atoms in the molecules.

In addition, certain compounds might have condensed onto pre-existing particles in the real atmosphere before an appreciable fraction of such compounds undergoes the re-initiated OH oxidation. Therefore, even the same product can be generated both in the laboratory experiments and the ambient atmosphere, the relative significance of this product is not completely identical. Though OOMs might have the potential to undergo multi-generation OH oxidation, the exact proportion of this reaction in the ambient strongly depends on their volatility, in other words, condensation sink of these OOMs. The typical monomeric termination products of 1,3,5-TMB-derived BPR, $C_9H_{12}O_4$, $C_9H_{14}O_4$, $C_9H_{14}O_5$, and $C_9H_{13}NO_6$, are estimated to have saturation vapor concentrations (C*) of 30.20, 30.20, 0.85, and 3.39 μg/m$^3$ at 300 K with the volatility parameterization developed in the CLOUD chamber oxidation experiments of aromatics, respectively (Wang et al., 2020a). From the perspective of volatility, they all belong to semi-volatile organic compounds (SVOC, $0.3 < C^* < 300$ μg/m$^3$) and are expected to exist in both the condensed and the gas phases at equilibrium in the atmosphere (Bianchi et al., 2019). Compared to ambient conditions, their condensation rates in the laboratory were biased to be lower due to the accelerated bimolecular reactions. However, this will not prevent the high [OH] experiments from showing the potential and ability of these compounds to go through re-initiated OH oxidation, as these compounds would exist in significant fractions in the gas phase in the real atmosphere.

However, the conditions are completely distinct for other HOM monomer products and HOM dimer products with much lower volatility. It is difficult for a HOM dimer, e.g., $C_{18}H_{26}O_{10}$ estimated with a C* of $7.24\times10^{-13}$ μg/m$^3$ at 300 K, to survive long enough to experience an appreciable re-initiated photochemical ageing. The lifetime of HOMs that can be classified as LVOCs ($3\times10^{-5}$ < C* < 0.3 μg/m$^3$) and ELVOCs (C* < $3\times10^{-5}$ μg/m$^3$) can be estimated according to the condensation sink (CS) in the atmosphere, as they are lost irreversibly onto surfaces. The median value of CS in urban Beijing was reported to be around 0.019 s$^{-1}$ and 0.057 s$^{-1}$ during NPF days and non-NPF days, respectively, whereas the values in Shanghai were reported to be around 0.013 s$^{-1}$ and 0.017 s$^{-1}$. respectively (Deng et al., 2020; Yao et al., 2018), which are all much higher than the physical loss in our PAM OFR, i.e., 0.0023 s$^{-1}$, as stated in the Supplementary Text S1. LVOCs and ELVOCs are believed to be lost irreversibly to the surface in both the laboratory and ambient because of their low volatility. However, by assuming a similar diffusion coefficient of LVOCs and ELVOCs to that of sulfuric acid, the lifetimes of LVOCs and ELVOCs in the ambient still can be as high as 77 s for the condensation loss, which is close to the residence time of our PAM OFR. Therefore, LVOCs and ELVOCs should at least have the potential to experience the same OH exposures in the ambient as those in our low [OH] experiments, i.e., at least $5.86\times10^{8}$ molecule cm$^{-3}$ s, if they were generated. On the other hand, the detailed proportions of LVOCs and ELVOCs after a large OH exposure should be lower than those in the lab due to their magnified physical loss in the ambient. This means that if the multi-generation products of those compounds were observed in the ambient air, they should have been generated via a reaction that happened very recently.

### 3.2 Oxidation products in high [OH] experiments

A total of 33 HOM monomers with formulae of $C_{7-9}H_{8-16}O_{6-11}$ and 22 HOM dimers with formulae of $C_{17-18}H_{24-30}O_{8-14}$ were observed in the 1st-round experiments of gas phase OH-initiated oxidation of 1,3,5-TMB in the OFR, i.e., high [OH] experiments, as listed in Table S5. The relative signal contributions of HOMs to the total signals of all HOMs at an OH exposure of $2.38\times10^{10}$ molecules cm$^{-3}$ s are listed as an example in Table S5. The most abundant HOM products were also shown in stack in Figure 2, whose relationships with OH exposures are superimposed by a gamma function ($f(x) = ax^{m}e^{-x}$) simulation line to guide the eyes. The sum of normalized HOM monomers' abundance increased monotonically up to the highest OH exposure of $5\times10^{10}$ molecule cm$^{-3}$ s, whereas those of HOM dimers showed a non-monotonic dependence on OH exposure. The observed faster increase of accretion products than that of

HOM monomers can be explained jointly by the fast second-order kinetics for accretion reactions of $RO_2$ (Berndt et al., 2018b) and the high concentrations of relevant radicals in this work. On the other hand, most of the first-generation HOM dimers formed from accretion reactions contain at least one C=C bond and have more functionalities than HOM monomers, and thus should be more reactive to OH radicals, which, together with a faster deposition loss of dimers, results in a faster consumption of HOM dimers than monomers in the OFR. The faster production and consumption of HOM dimers allowed their concentrations to summit at middle levels of OH exposures. As stated in Section 3.1, because of the inherent disadvantage of laboratory experiments, [$RO_2$] is always too high in the OFR, which has been pointed out in a previous study (Bianchi et al., 2019). The accretion reactions in the OFR are relatively more significant than it should be in the ambient atmosphere. We do not mean to compare HOM monomer and HOM dimer signals crossly here, but to pay attention to their formulae.

(a)

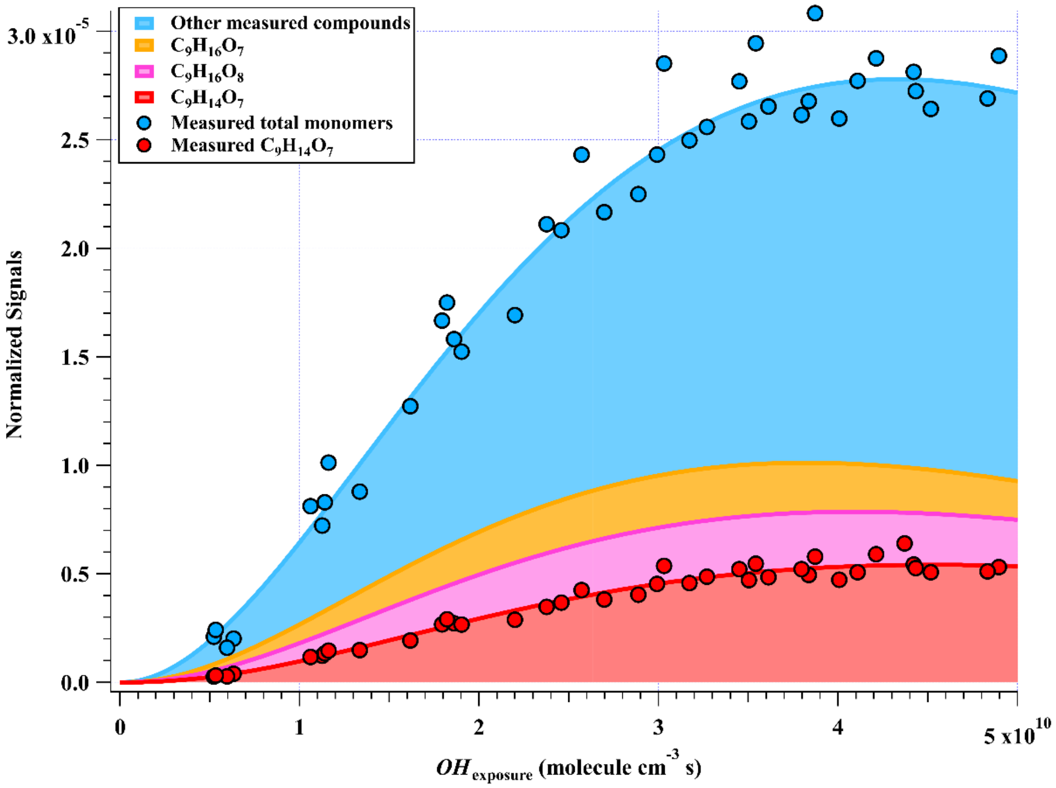

(b)

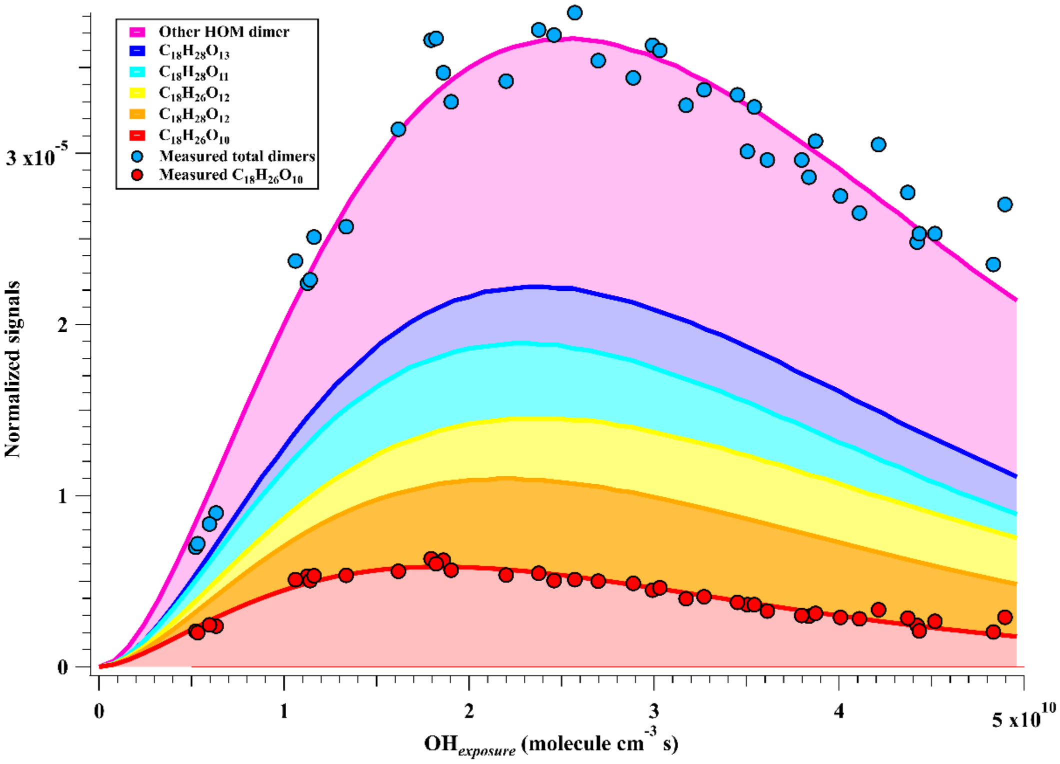

**Figure 2.** Normalized signals of (a) HOM monomers and (b) HOM dimers versus OH exposure in the high [OH] experiments, which are fitted via a gamma function and shown in stack.

Theoretically, at a given RH and UV (i.e., a given [OH]), an increase in the initial TMB would lead to formation of more $RO_2$, which corresponds to a larger $RO_2$/OH. However, under our high [OH] experimental conditions, the $RO_2$/OH/$HO_2$ channels of $RO_2$ radicals are always minor, and thus an increase in $RO_2$/OH would not have a significant impact on the relative distribution of products formed from these channels. We compared product MS for experiments with a similar OH exposure but different initial concentrations of TMB (e.g., Exp. 1-3 v.s. Exp. 1-19, and Exp. 1-12 v.s. Exp. 1-22). The OH exposures of Exp. 1-3 and Exp. 1-19 were estimated by the consumption of precursors to be $5.2 \times 10^9$ and $5.3 \times 10^9$ molecule $cm^{-3}$ s, respectively, but the initial concentration of TMB of Exp. 1-3 was 25% more than that in Exp. 1-19. Meanwhile, the OH exposures of Exp. 1-12 and Exp. 1-22 were $4.5 \times 10^{10}$ and $4.4 \times 10^{10}$ molecule $cm^{-3}$ s, respectively, but the initial concentration of TMB of Exp. 1-12 was 48% more than that in Exp. 1-22. Comparisons between the product MS of Exp. 1-3 and Exp. 1-19 (Figure S2), as well as of Exp. 1-12 and Exp. 1-22, show that increase in the initial concentration of precursors generally resulted in a minor increment in the absolute signals of HOMs. Clearly, the relative distributions of products in these experiments are quite similar, indicating a minor difference in the relative distributions of products caused by fluctuations of initial concentrations of TMB.

### 3.2.1 HOM monomers

Previous studies indicate that oxidation products derived from the peroxide-bicyclic pathway represent a main fraction of HOMs (Wang et al., 2017; Zaytsev et al., 2019). For 1,3,5-TMB, this pathway, as recommended by Master Chemical Mechanism (MCM), starts from a BPR, $C_9H_{13}O_5\cdot$ (MCM name: TM135BPRO2) (Molteni et al., 2018). According to MCM and Molteni et al. (2018), Scheme 1 has been proposed to provide a good understanding of this reaction system and the structures of oxidation products. Molteni et al. (2018) suggested that $C_9H_{13}O_7\cdot$, i.e., peroxy radical formed from autooxidation of $C_9H_{13}O_5\cdot$ has two isomers. A second-step of endo-cyclization is required in the formation of one of the isomer, which is extremely slow and not competitive as shown in several previous studies using both experimental and theoretical approaches (Wang et al., 2017; Xu et al., 2020). Even if such a second $O_2$ bridging to a double bond is assumed to be possible, the abundance of this isomer should be significantly smaller than the other one, because of the much faster reaction rate of H-shift reaction. Therefore, we do not take the $C_9H_{13}O_7\cdot$ isomer containing a double endo-cyclization into consideration in this work. The majority of HOM monomers is generated from subsequent reactions of $C_9H_{13}O_5\cdot$ and newly formed $C_9H_{13}O_7\cdot$, both of which contain one C=C bond in the carbon backbone and thus have a feasible site for OH addition. Meanwhile, the autoxidation reaction rate for newly formed $C_9H_{13}O_7\cdot$ should be significantly smaller than $C_9H_{13}O_5\cdot$, as there is no hydrogen atom in $C_9H_{13}O_7\cdot$ that is able to undergo a hydrogen atom shift at an appreciable rate based on our current understanding. Therefore, the subsequent autoxidation reaction should not be able to generate large amounts of more oxidized $RO_2$.

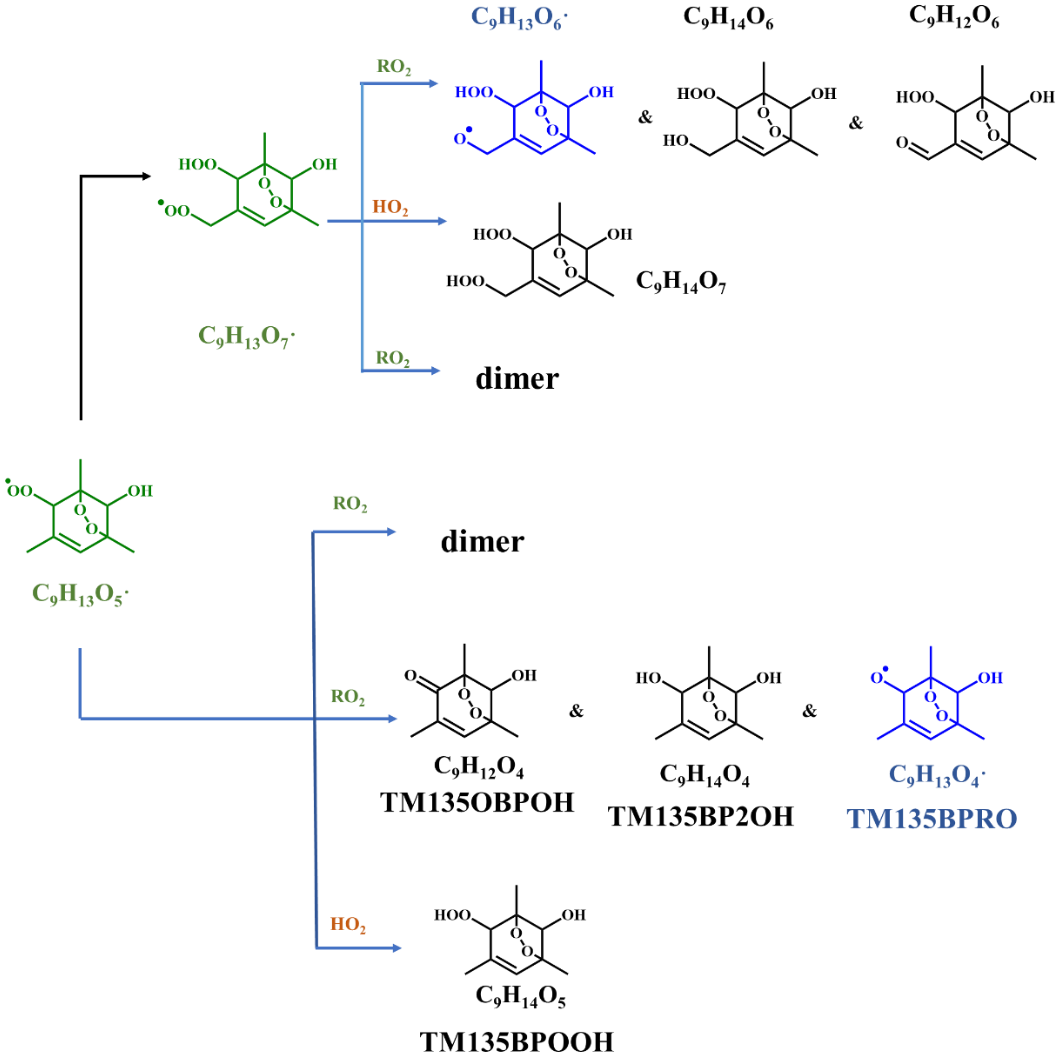

**Scheme 1.** Oxidation pathways of the bicyclic peroxy radical $C_9H_{13}O_5\cdot$ (MCM name: TM135BPRO2) in the OH-initiated oxidation of 1,3,5-TMB. Green, blue, and black formulae denote alkyl peroxy radicals, alkoxy radicals and stabilized products, respectively. Black arrows denote the autoxidation pathway. MCM names for $HO_2$- and $RO_2$-termination products of TM135BPRO2 are present.

Monomeric termination products of BPR, as shown in Scheme 1, were not detected by nitrate CIMS in this round of experiments, which might be due to the fast sub-sequential OH oxidation of these products under high [OH] environment since they were observed under low [OH] environments as shown in Section 3.3. Monomeric termination products of $C_9H_{13}O_7\cdot$ were all observed clearly, including $C_9H_{12}O_6$, $C_9H_{14}O_6$, and $C_9H_{14}O_7$. Especially, $C_9H_{14}O_7$ was the most abundant one among all of the HOM monomer products (Figure 2a). As proved by a previous study, these three species should be typical first-generation stabilized products derived from autoxidation (Wang et al., 2020b). These HOM monomers should consist of several isomers bearing the same formula, because products from the secondary reactions cannot share the same structure as that of the one from the first-generation reaction. However, limited by the inherent disadvantages of mass spectrometers, we could not distinguish isomers here and further illustrate their different chemical behaviors.

In addition to these three ones, the next most prominent products to $C_9H_{14}O_7$ were $C_9H_{16}O_7$ and $C_9H_{16}O_8$ (Figure 3a), which are produced from multi-generation oxidation according to their DBE. Based on the formulae of these three HOM monomers, they ($C_9H_{14}O_7$, $C_9H_{16}O_7$, and $C_9H_{16}O_8$) could be formed from the bimolecular termination reactions of $C_9H_{15}O_8\cdot$, which can be generated by an OH attack to $C_9H_{14}O_5$ (Scheme 2), the hydroperoxyl termination product of the BPR, $C_9H_{13}O_5\cdot$. The other HOM monomers characterized with high signals were $C_9H_{14}O_8$ and $C_9H_{16}O_9$ (Figure 3b). These two HOM monomers ($C_9H_{14}O_8$ and $C_9H_{16}O_9$), together with $C_9H_{16}O_8$, correspond to the monomeric termination products of $C_9H_{15}O_9\cdot$, which is highly likely the peroxy radical generated by an OH attack to $C_9H_{14}O_6$ (Scheme 3), i.e., the hydroxyl termination product of $C_9H_{13}O_7\cdot$. As discussed earlier, $C_9H_{13}O_7\cdot$ is a typical autoxidation reaction product of the BPR of $C_9H_{13}O_5\cdot$. Therefore, detected signals of $C_9H_{16}O_8$ should be the sum of two isomers' signals at least. Other HOM monomers were generally observed at much lower signals and thus were not plotted individually.

(a)

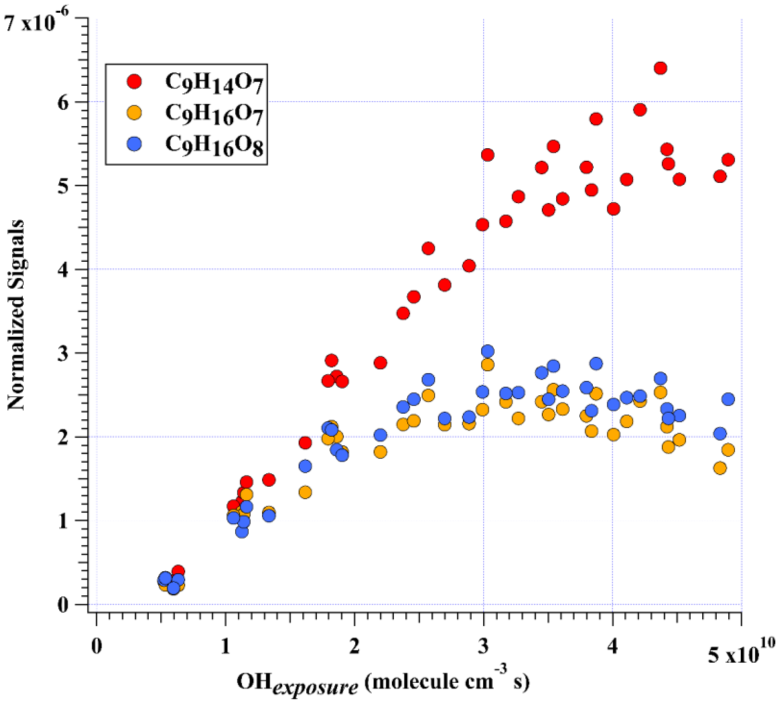

(b)

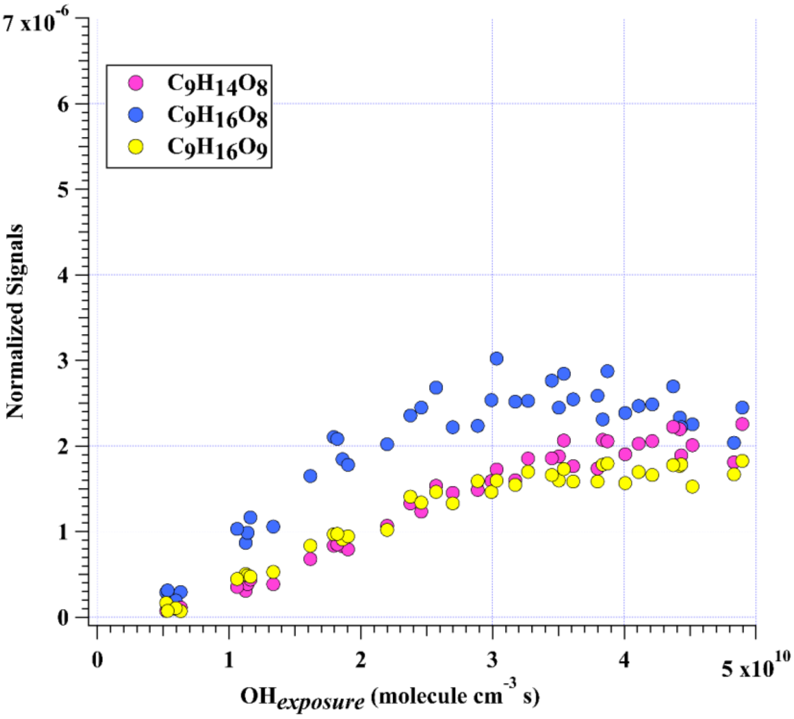

**Figure 3.** Normalized signals of (a) $C_9H_{14}O_7$, $C_9H_{16}O_7$, and $C_9H_{16}O_8$ and (b) $C_9H_{14}O_8$, $C_9H_{16}O_8$, and $C_9H_{16}O_9$ measured at the exit of OFR in our high [OH] experiments without $NO_x$ as a function of OH exposure. $C_9H_{16}O_8$ are shown in both plots to better illustrate the chemical profiles of different compound groups.

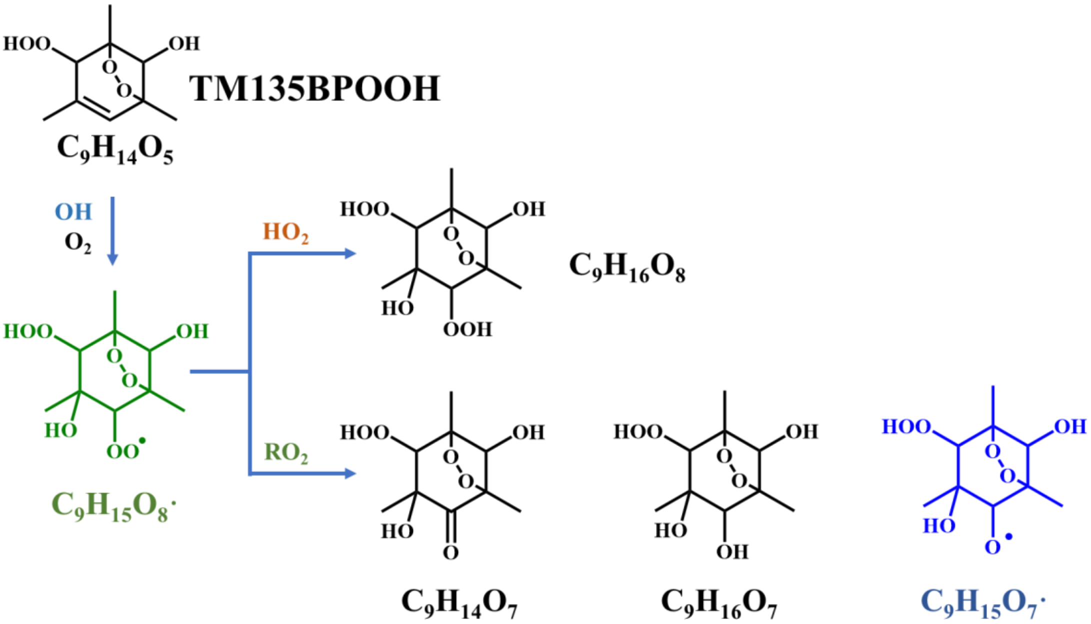

**Scheme 2.** Proposed formation pathways of $C_9H_{14}O_7$, $C_9H_{16}O_7$, and $C_9H_{16}O_8$ via the secondary OH oxidation of TM135BPOOH.

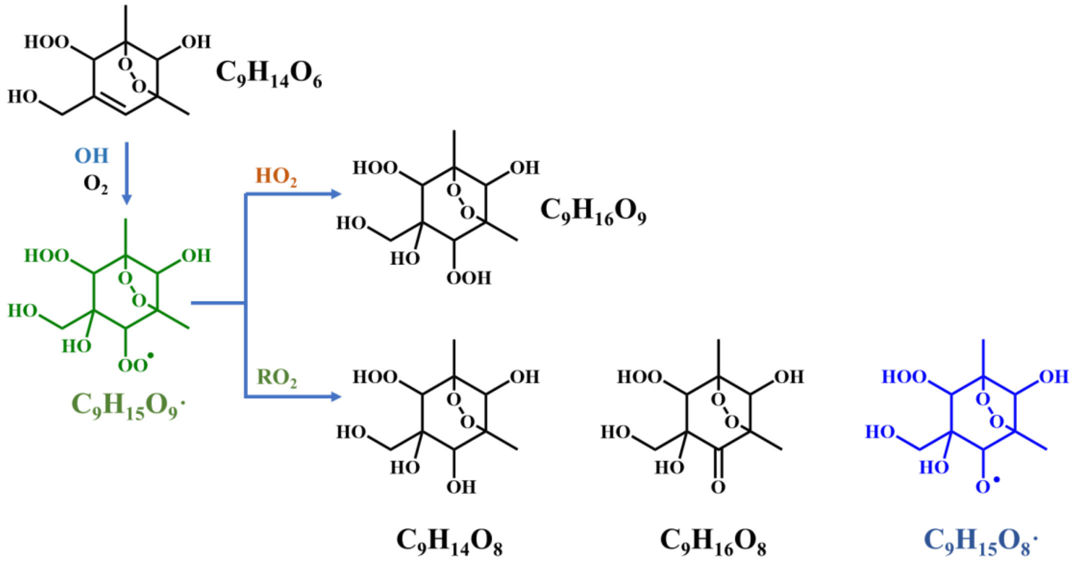

**Scheme 3.** Proposed formation pathways of $C_9H_{14}O_8$, $C_9H_{16}O_8$, and $C_9H_{16}O_9$ via the secondary OH oxidation of TM135BPOOH.

It is worth noting that HOM monomers with 18 hydrogen atoms, i.e., a DBE of 1, were never observed in our experiments, including a potential stabilized hydroperoxyl products formed from $C_9H_{17}O_m\cdot$. This is expected, since $C_9H_{17}O_m\cdot$ should be in really low concentrations, if ever existed. As indicated by its hydrogen number, a $C_9H_{17}O_m\cdot$ was formed by at least two OH additions to the C=C bond of a $C_9H_{13}O_m\cdot$, but the main BPR, $C_9H_{13}O_5\cdot$, and its autoxidation product ($C_9H_{13}O_7\cdot$), are characterized with one C=C bond on the ring, which makes this formation pathway impossible. Other ring-breakage pathways should not contribute to the formation of this radical ($C_9H_{17}O_m\cdot$) because of their low branching ratio as determined by recent studies (Zaytsev et al., 2019; Xu et al., 2020).

Proposed according to MCM and Molteni et al. (2018), scheme 4 shows the NO termination pathways of the main BPR $C_9H_{13}O_5\cdot$ and its autoxidation product, $C_9H_{13}O_7\cdot$. After introducing $N_2O$ into PAM OFR, quantities of organonitrates were generated, including both C9 and C18 organonitrates. The averaged mass spectrometry of nitrate CIMS in the 1.8 ppb NO experiment and 4.8 ppb NO experiment is shown in Figure S3. Organonitrates were formed via the NO + $RO_2$ reaction, called as NO termination reactions. The distribution of oxidation products under these two NO settings were similar.

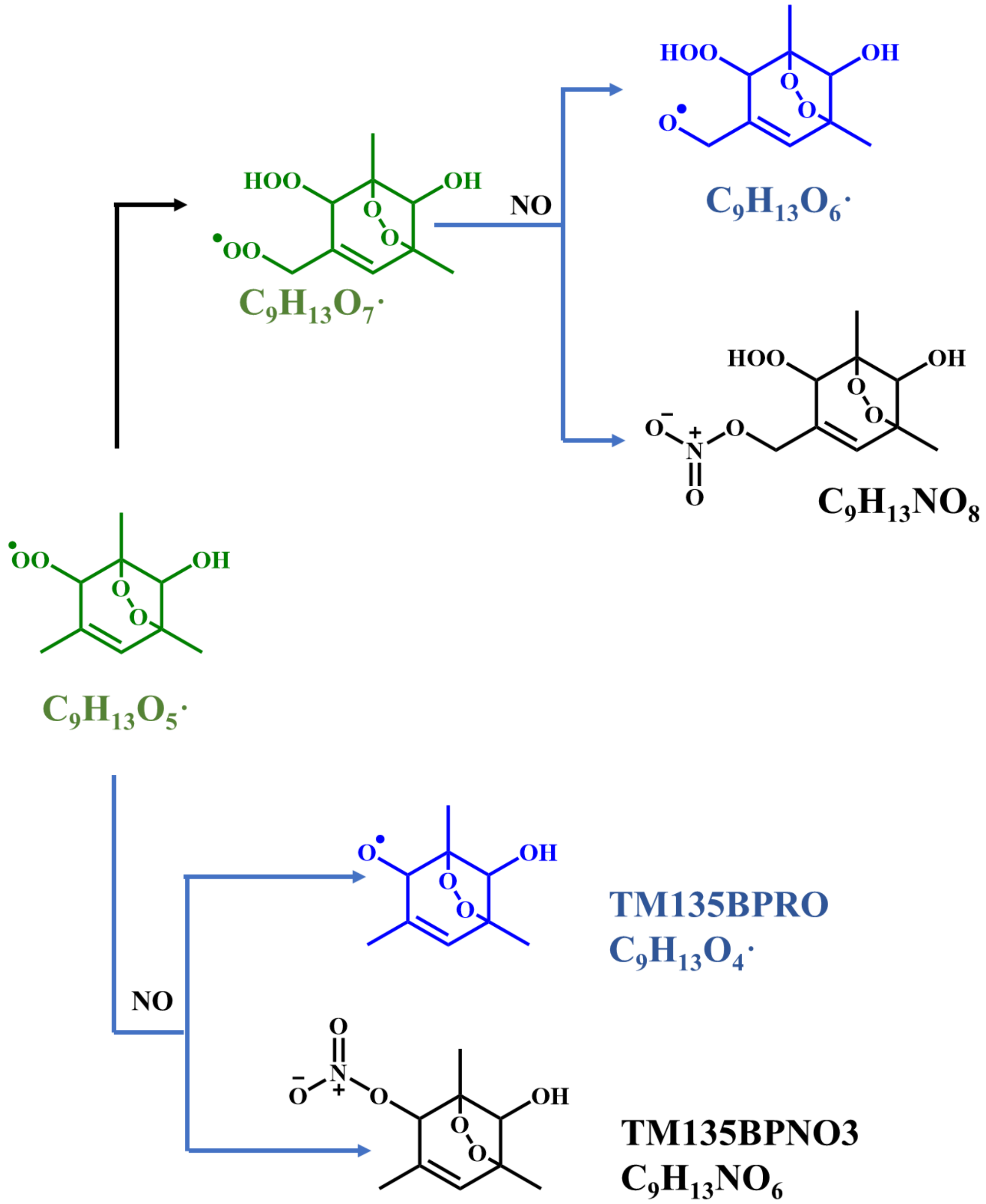

**Scheme 4**. NO termination reactions of the bicyclic peroxy radical $C_9H_{13}O_5\cdot$ (MCM name: TM135BPRO2) and its autoxidation reaction products. Green, blue, and black formulae denote alkyl peroxy radicals, alkoxy radicals and stabilized products, respectively. Black arrows denote the autoxidation pathway. MCM names of NO-termination products of TM135BPRO2 are present.

As discussed above, most of the first-generation HOMs should contain a C=C bond in the carbon backbone. The ubiquitous existence of organonitrates that contain two nitrogen atoms exactly confirms the extensive secondary OH oxidation in the systems, because the NO termination reaction of $RO_2$ is the only pathway that can generate organonitrates in our experiments and this pathway can only introduce one nitrogen atom at a time, as indicated in Scheme 4. $RO_2$ can react with $NO_2$ to form peroxynitrates ($ROONO_2$) but these species are thermally unstable except at very low temperatures or when the $RO_2$ is an acylperoxy radical (Orlando and Tyndall, 2012), neither of which were not met in our experiments. The concentrations of $NO_3$ were estimated to be lower than 1 pptv by our modified PAM_chem_v8 because of the existence of decent concentrations of NO, which would consume $NO_3$ at a rapid reaction rate, i.e., $2.7\times10^{-11}$ molecule$^{-1}$ cm$^3$ s$^{-1}$ (IUPAC dataset , https://iupac-aeris.ipsl.fr, last access: 26 October 2023). Therefore, $NO_2$ and $NO_3$ were not likely to react with $RO_2$ to form large amounts of organonitrates in our experiments. Taking the most abundant organonitrate, $C_9H_{14}N_2O_{10}$, as an example, it was exactly the NO termination product of $C_9H_{14}NO_9\cdot$, which was generated from an OH attack and a subsequent $O_2$ addition to $C_9H_{13}NO_6$, the NO termination product of $C_9H_{13}O_5\cdot$. For other organonitrates, $C_9H_{13}NO_8$, the second most abundant organonitrate, could be either a NO termination product of $C_9H_{13}O_7\cdot$ or, together with other most abundant organonitrates, $C_9H_{15}NO_7$ and $C_9H_{15}NO_8$, classical termination products of $C_9H_{14}NO_9\cdot$. $C_9H_{14}N_2O_{10}$, $C_9H_{15}NO_7$, and $C_9H_{15}NO_8$ all have a DBE of 2 lower than the precursor and thus are the typical multi-generation OH oxidation products.

The NO:$RO_2$ ratio in the PAM OFR in this series of experiments is lower than typical values in the ambient atmosphere, which is due to the existence of $O_3$ that was utilized to generate $O(^1D)$ in the OFR and its rapid reaction rate with NO. However, due to rapid reaction rate constants between NO and $RO_2$, i.e., around $8.5\times10^{-12}$ molecule$^{-1}$ cm$^3$ s$^{-1}$, the reaction rate for the NO termination channel of $RO_2$ was as fast as around 0.3 – 1.0 s$^{-1}$. Large amounts of organonitrates would still be formed, as discussed in Section 3.1. Our conclusion is also valid because of detection of compounds with multiple nitrogen atoms.

### 3.2.2 HOM dimers

Accretion reaction $\mathrm{RO_2 + RO'_2 \rightarrow ROOR' + O_2}$ is a source of gas-phase dimer compounds from highly oxidized, functional $RO_2$ radicals (Ehn et al., 2014; Berndt et al., 2018b; Zhao et al., 2018; Berndt et al., 2018a). $C_{18}H_{26}O_8$ and $C_{18}H_{26}O_{10}$ are two typical accretion reaction products in the 1,3,5-TMB + OH system, whose formation pathways have been elucidated (Berndt et al., 2018b). $C_{18}H_{26}O_8$ can only be formed via the accretion reaction of two $C_9H_{13}O_5\cdot$. $C_9H_{13}O_3\cdot$ is not likely to react with $C_9H_{13}O_7\cdot$ to form large amounts of $C_{18}H_{26}O_8$. $C_9H_{13}O_3\cdot$ can only be formed after addition of a hydroxyl radical to the aromatic ring of 1,3,5-TMB and a subsequent $O_2$ addition to the newly formed hydroxyl-substituted cyclohexadienyl radical (Vereecken, 2019). However, the lifetime of this radical is extremely short, as $C_9H_{13}O_3\cdot$ will undertake a ring-closure reaction and get attached by a $O_2$ very rapidly, forming BPR, $C_9H_{13}O_5\cdot$. Its short lifetime and low concentration, as indicated by Berndt et al. (2018), lead to its insignificant role in the accretion reactions. In contrast, $C_{18}H_{26}O_{10}$ can be formed either by the accretion reaction between $C_9H_{13}O_5\cdot$ and $C_9H_{13}O_7\cdot$or via a second OH attack to $C_{18}H_{26}O_8$.

These two HOM dimers are so far the only ones that are confirmed to be formed via the accretion reactions (Berndt et al., 2018b; Bianchi et al., 2019).

$C_{18}H_{26}O_{10}$ was characterized with the highest dimer signals for experiments with OH exposures under $3.5\times10^{10}$ molecule cm$^{-3}$ s. Nevertheless, $C_{18}H_{26}O_{10}$, together with $C_{18}H_{28}O_{12}$, $C_{18}H_{26}O_{12}$, $C_{18}H_{28}O_{11}$, $C_{18}H_{28}O_{13}$, and $C_{18}H_{28}O_{10}$ contributed more than 50% of total HOM dimer signals at any OH exposure levels (Figure 2b). These six most abundant HOM dimers correspond exactly to the hydroperoxyl, hydroxyl, and carbonyl termination products of $C_{18}H_{27}O_{11}\cdot$ and $C_{18}H_{27}O_{13}\cdot$, respectively. These two $RO_2$ ($C_{18}H_{27}O_{11}\cdot$ and $C_{18}H_{27}O_{13}\cdot$), on the other hand, could be generated by OH attacks to $C_{18}H_{26}O_8$ and $C_{18}H_{26}O_{10}$, respectively, which strongly suggests the significant role of secondary OH chemistry in the formation of HOMs in our experiments. In addition, $C_{18}H_{28}O_x$ can also be formed through accretion of a $C_9H_{13}O_m\cdot$ radical and a $C_9H_{15}O_m\cdot$ radical, as suggested by previous studies (Molteni et al., 2018; Tsiligiannis et al., 2019). However, since a $C_9H_{15}O_m\cdot$ radical, as suggested by its hydrogen atom number, can only be formed via an OH addition to the stabilized $C_9H_{14}O_m$ products through multi-generation OH reactions, our conclusion that $C_{18}H_{28}O_x$ are multi-generation OH oxidation products still holds. Figure 4 shows the normalized signals of these abundant HOM dimers at different OH exposures.

(a)

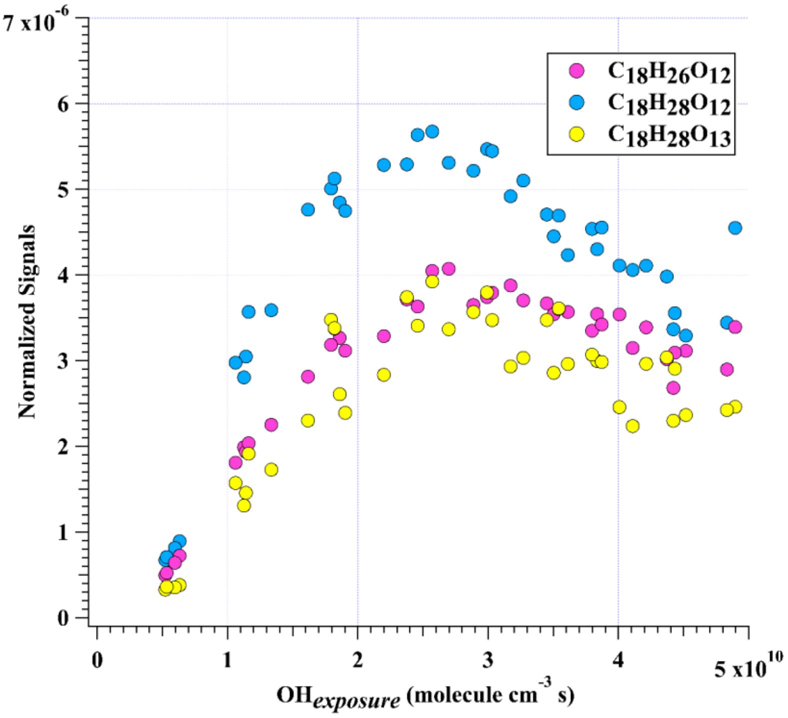

(b)

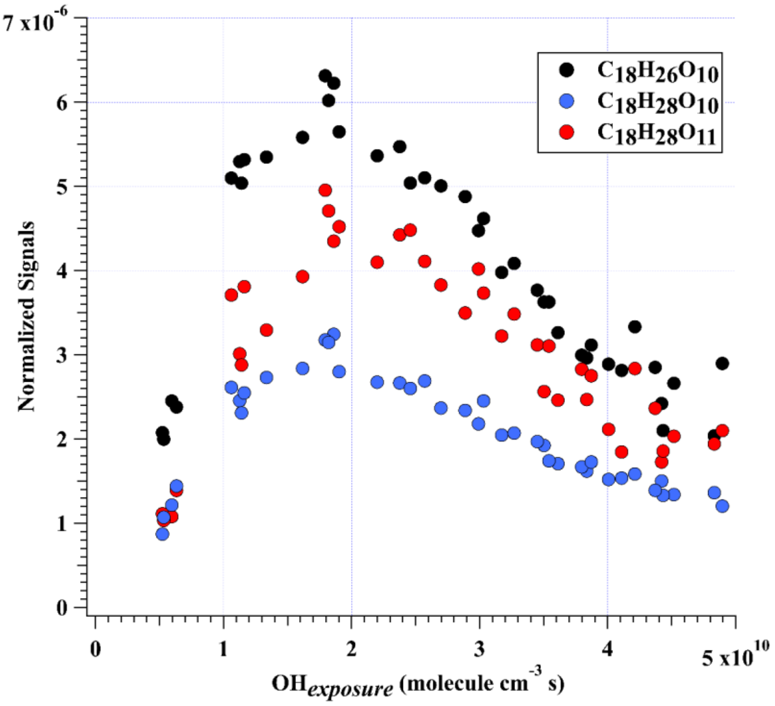

**Figure 4.** Normalized signals of (a) $C_{18}H_{26}O_{12}$, $C_{18}H_{28}O_{12}$, and $C_{18}H_{28}O_{13}$, and (b) $C_{18}H_{26}O_{10}$, $C_{18}H_{28}O_{10}$, and $C_{18}H_{28}O_{11}$ measured at the exit of OFR in our high [OH] experiments without $NO_x$ as a function of OH exposure.

This decrease of dimer at relatively high OH exposures are likely due to the accelerated accretion reactions in the OFR, resulted by the high $RO_2$ concentrations. The HOM dimers are formed earlier compared to under ambient conditions and then can go through the further oxidation reactions. Note that this does not mean the maximum concentrations of HOM dimers will also accurately occur at the same OH exposures in the atmosphere, because the detailed appearance time of the maximum concentrations of HOM dimers is dependent on their formation rate and loss rate. In our experiments, the formation rate and loss rate were not accelerated equally. On the other hand, the loss pathways of HOM dimers were not exactly the same as the ambient due to the lack of aerosols in the OFR. With the decrease of particulate pollution and thus condensation sinks in the polluted areas, the physical loss of HOMs might be lower and the chemical process can be more important. This series of experiments are not meant to specifically find out the detailed OH exposures when the maximum concentrations of HOM dimers will occur, but try to indicate how HOM dimers evolve with the increase of OH exposures. This work can be regarded as an indicator for the potential chemical fates of HOM dimers in the atmosphere if their survival time permitted. It should be noted that the gas-phase chemistry in the PAM OFR cannot be exactly the same as that in the ambient. Reactions of OH with OVOCs often lead to $HO_2$ formation, resulting in a $HO_2$:$RO_2$ ratio larger than 1 in the real atmosphere (Bianchi et al., 2019). A recent campaign conducted at a rural site in the Yangtze

River Delta estimated that the local ratio of $HO_2:RO_2$, the latter of which was presumably derived from longer chain alkanes (> $C_3$), alkenes, and aromatic compounds, was around 1.66 (Ma et al., 2022). Such a high $HO_2:RO_2$ ratio condition is typically difficult to be simulated in the laboratory experiments, as the precursors are usually hydrocarbons without any OVOCs (Peng and Jimenez, 2020). This is exactly the case for our experiments, but its influences on our conclusion were tiny, as have been discussed in the Section 3.1. Therefore, the difference in the distribution of products will not change our conclusion.

Such an active secondary OH chemistry is consistent with the fast OH reaction rates of HOMs. We take $C_{18}H_{26}O_8$ whose plausible structure is shown in Figure S4 as an example, which is the accretion product of two $C_9H_{13}O_5\cdot$. Its OH reaction rate constant is estimated to be around $2.07 \times 10^{-10}$ $cm^3$ $molecule^{-1}$ $s^{-1}$ according to the structure-activity relationship (Jenkin et al., 2018b, a), whose details are provided in Supplementary Text S2. This rate is several times larger than that of 1,3,5-TMB, which enables a very active secondary OH chemistry in the system. MCM recommended an OH reaction rate of $1.28 \times 10^{-10}$ $cm^3$ $molecule^{-1}$ $s^{-1}$ for TM135BPOOH ($C_9H_{14}O_5$) and $1.00 \times 10^{-10}$ $cm^3$ $molecule^{-1}$ $s^{-1}$ for TM135OBPOH ($C_9H_{12}O_4$) (Jenkin et al., 2003). The OH reaction rate for $C_{18}H_{26}O_8$ should also be fast due to the C=C bonds in its structure, which is activated by the adjacent functionalities. Our calculation result is consistent with this estimation.

The distributions of C18 organonitrates also verified the extensive secondary reactions. The most abundant C18 organonitrate, $C_{18}H_{27}NO_{12}$ was a NO termination product of radical $C_{18}H_{27}O_{11}\cdot$, which, as mentioned above, was the radical generated from the OH reaction with $C_{18}H_{26}O_8$. $C_{18}H_{27}NO_{12}$ can also be formed either by accretion between a $C_9H_{15}O_m\cdot$ radical and a $C_9H_{12}NO_m\cdot$ radical or accretion between a $C_9H_{13}O_m\cdot$ radical and a $C_9H_{14}NO_m\cdot$ radical. Both $C_9H_{15}O_m\cdot$ and $C_9H_{14}NO_m\cdot$ radicals are a typical multi-generation $RO_2$ and thus prove $C_{18}H_{27}NO_{12}$ is a multi-generation OH oxidation product. Other C18 organonitrates are believed to be formed in a similar pathway. Hence, plenty of organonitrates have been formed via the multi-generation OH reactions of first-generation stabilized products.

## 3.3 Oxidation products in low [OH] experiments

Given the larger sampling port, lower initial ozone concentrations, lower UV light intensities, and a better performance of mass spectrometer in this series of low [OH] experiments, a number of new species were detected in the 2nd-round experiments, including three typical termination reaction products of BPR, i.e., $C_9H_{14}O_4$, $C_9H_{14}O_5$, and $C_9H_{13}NO_6$, and a number of low volatile compounds, e.g., $C_9H_xO_{11}$ ($x$ = 12 - 15). The distributions of oxidation products detected by nitrate CI-TOF in Exp. 2-3, 2-4, and 2-7, representative low [OH] experiments, are displayed in Figure 5. The detailed molecular formula and their contributions to total HOMs signals are provided in Tables S6 and S7.

In addition, certain C9 and C18 HOMs with lower DBE than typical first-generation products predicted by MCM (Saunders et al., 2003) or reported by previous studies (Berndt et al., 2018b), were detected in Exp. 2-3, 2-4, and 2-7, although [OH] in these experiments are much lower than those in the 1st-round experiments.

Observation of compounds with lower DBE in Exp. 2-3, 2-4, and 2-7 including HOM monomers with DBE lower than 3 and HOM dimers with DBE lower than 6, as well as monomer radicals with DBE lower than 3 including $C_9H_{15}O_m\cdot$ ($m$ = 7 - 11) and $C_9H_{14}NO_9\cdot$, proves the re-initiation of OH oxidation of the stabilized products in experiments with atmospheric relevant [OH]. All the stabilized products and radicals depicted in the proposed mechanisms (Scheme 2 and Scheme 3) were detected in both Exp. 2-3 and Exp. 2-4, except for $C_9H_{15}O_9\cdot$ that was only detected in Exp. 2-3. This means that the proposed reaction pathways have already happened under atmospheric [OH] conditions with limited OH exposures. However, as we do not know the exact structures of these OOMs and radicals, the proposed reaction pathways are merely based on the chemical formulae detected by nitrate CIMS and nitrate CI-TOF and proposed according to the general mechanisms of OH addition reactions to the C=C bond. Other reaction pathways to generate these compounds or other isomers generated in these pathways are undoubtedly feasible.

A lot of compounds detected in the experiments without $NO_x$ were not observed in counterpart experiments with $NO_x$. We also did not detect decent signals of HOM dimers in the $NO_x$-present experiments in the 2nd-round experiments. This might come from the dominant significance of NO + $RO_2$ reactions ($R8$ - $R9$) after the introduction of $NO_x$ into system, making signals of certain HOMs from other channels lower than the detection limit of the instrument. The proportions of other reaction channels decreased, and were reassigned to the NO channel, as evidenced by the fact that most of observed oxidation products were organonitrates, which is in an excellent agreement with the modeled channel proportions in Section 3.1.

Many organonitrates were observed in both series of experiments In the low [OH] experiments, the most significant compound was $C_9H_{13}NO_8$, whose formula matches the NO termination product of $C_9H_{13}O_7\cdot$, i.e., autoxidation product of BPR. The second most important compound, $C_9H_{14}N_2O_{10}$ in our low [OH] experiments, was the most significant product in the high [OH] experiments in presence of $NO_x$, whose formula matches the NO termination product of $C_9H_{14}NO_9\cdot$, i.e., the $RO_2$ formed via an OH addition to $C_9H_{13}NO_6$, the NO termination product of BPR. All of the products and radicals mentioned above were observed in Exp. 2-7, as shown in Figure 5c. From the perspective of molecular formula, $C_9H_{14}N_2O_{10}$ is also one of the most frequently observed multi-nitrogen-containing compound in polluted atmospheres, whose seasonal variations show a good correlation with [OH] (Guo et al., 2022; Yang et al., 2023).

A comparison of relative abundances of C9 and C18 products under different [OH] levels is helpful for the elucidation of their formation pathways. The difference in product distributions between Exp. 2-3 ([OH] = ~$1.69\times10^{7}$ molecule $cm^{-3}$) and Exp. 2-1 ([OH] = ~$1.03\times10^{8}$ molecule $cm^{-3}$), as well as between Exp. 2-3 and Exp. 1-12 ([OH] = ~$8.47\times10^{8}$ molecule $cm^{-3}$) is shown in Figure 6. The normalized abundance was obtained by normalizing all the products to the most abundant one in each experiment, i.e., $C_{18}H_{26}O_{10}$ in Exp. 2-1 and Exp. 2-3, and $C_9H_{14}O_7$ in Exp. 1-12. The changes in the normalized abundance were obtained by subtracting the normalized abundance in Exp. 2-1 from that in Exp. 2-3, and Exp. 1-12 from Exp. 2-3. As the [OH] and OH exposure increased, there was a noticeable rise in the relative abundance of more oxygenated compounds, which can be attributed to the more intensive proportion of multi-generation OH oxidation in high OH exposure experiments. This comparison demonstrates the capacity and potential of multi-generation OH oxidation to reduce DBE and elevate the oxygenated levels of oxidation products.

In conclusion, observation of the same low DBE compounds, i.e., DBE = 2, in both low [OH] and high [OH] experiments confirms the feasibility of the generation of HOMs under atmospheric relevant conditions. The detection of $C_9H_{14}O_5$, $C_9H_{15}O_8\cdot$, $C_9H_{14}O_7$, $C_9H_{14}O_8$, $C_9H_{15}O_7\cdot$, and $C_9H_{16}O_8$, and $C_9H_{14}O_6$, $C_9H_{15}O_9\cdot$, $C_9H_{14}O_8$, $C_9H_{14}O_9$, $C_9H_{15}O_8\cdot$, and $C_9H_{16}O_9$, in low [OH] experiments also confirms the potential existence of the proposed mechanisms, i.e., Scheme 2 and Scheme 3, respectively. Certainly, other potential formation pathways for these products are possible.

**(a)**

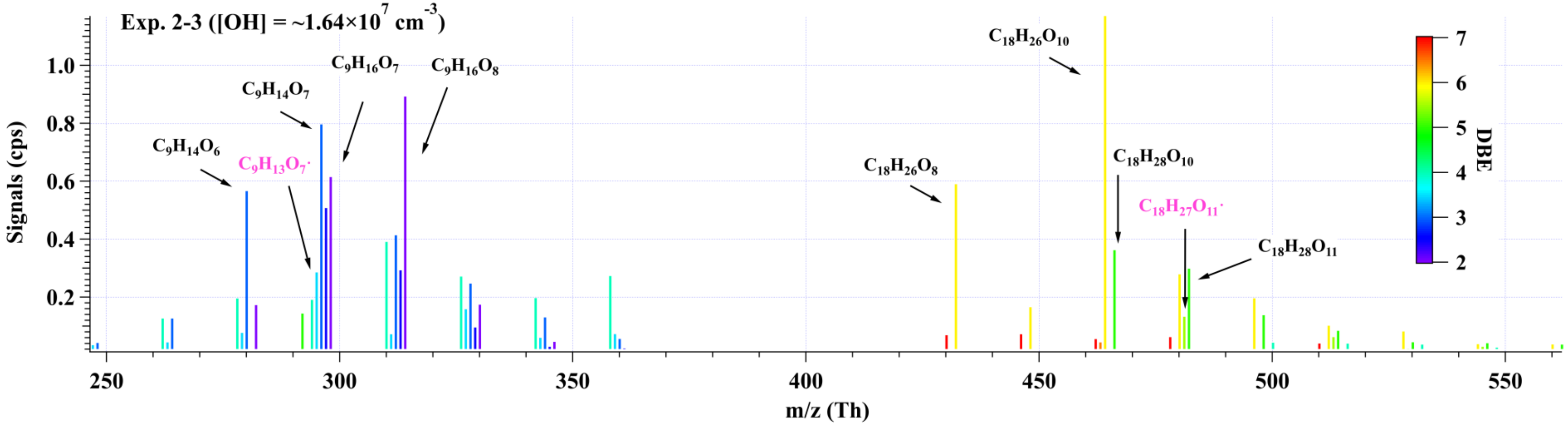
Exp. 2-3 ([OH] = ~1.64×10^7 cm^-3)
Signals (cps)
1.0
0.8
0.6
0.4
0.2
$C_9H_{14}O_6$
$C_9H_{13}O_7\cdot$
$C_9H_{14}O_7$
$C_9H_{16}O_7$
$C_9H_{16}O_8$
$C_{18}H_{26}O_8$
$C_{18}H_{26}O_{10}$
$C_{18}H_{28}O_{10}$
$C_{18}H_{27}O_{11}\cdot$
$C_{18}H_{28}O_{11}$
DBE
7
6
5
4
3
2
250
300
350
400
450
500
550
m/z (Th)

**(b)**

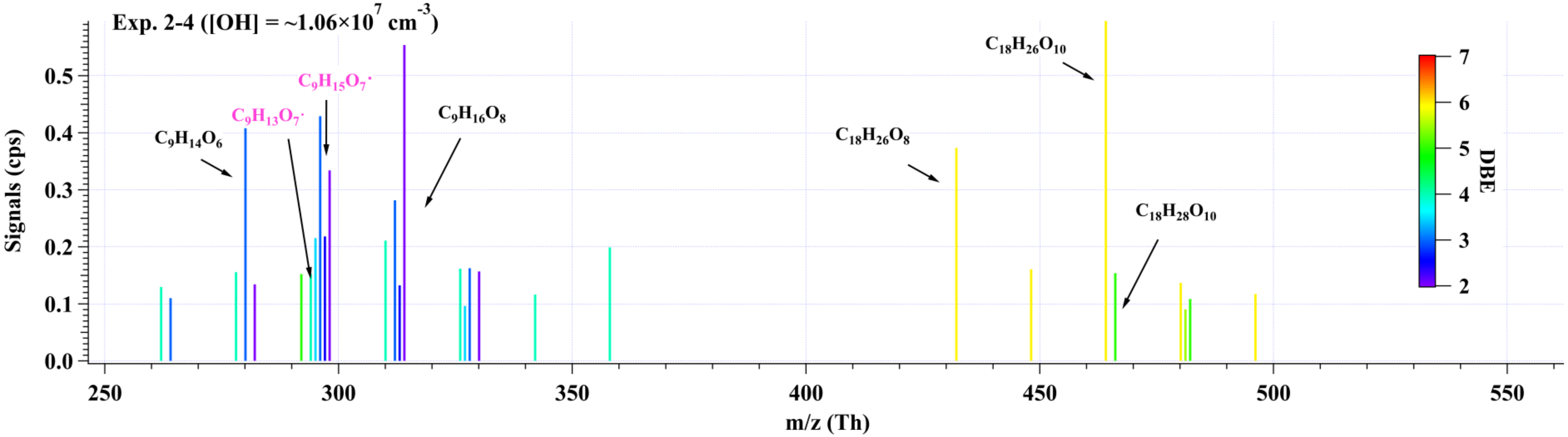
Exp. 2-4 ([OH] = ~1.06×10$^{7}$ cm$^{-3}$)
$C_9H_{14}O_6$
$C_9H_{13}O_7^{\cdot}$
$C_9H_{15}O_7^{\cdot}$
$C_9H_{16}O_8$
$C_{18}H_{26}O_8$
$C_{18}H_{26}O_{10}$
$C_{18}H_{28}O_{10}$
Signals (cps)
0.0
0.1
0.2
0.3
0.4
0.5
m/z (Th)
250
300
350
400
450
500
550
DBE
2
3
4
5
6
7

794

(c)

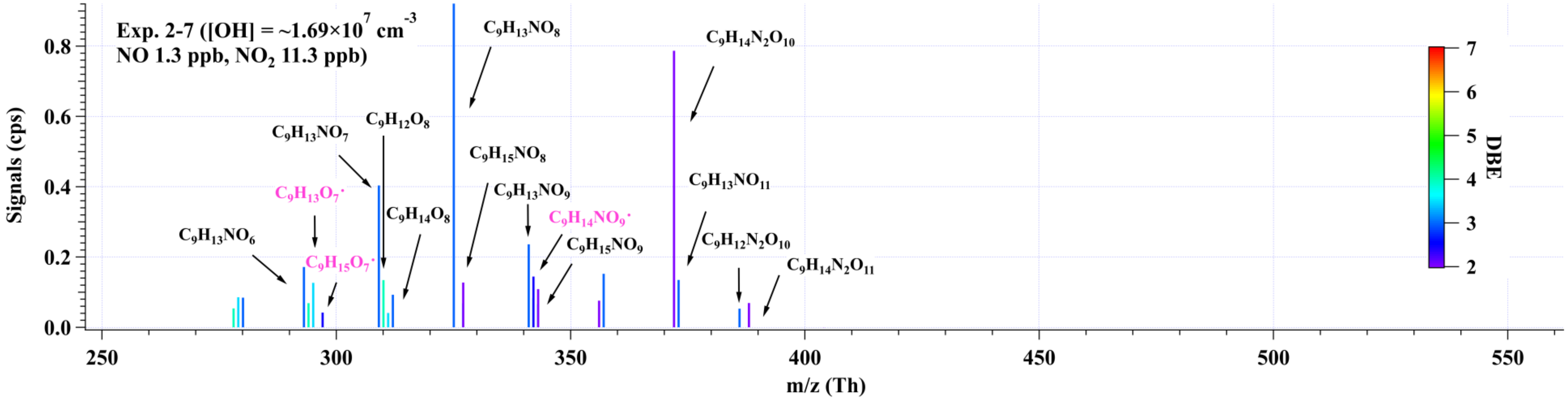

**Figure 5.** Distributions of C9 and C18 products detected by nitrate CI-TOF in (a) Exp. 2-3, (b) Exp. 2-4, and (c) Exp. 2-7. The reagent ion, $NO_3^-$, is omitted in the label for the molecular formula. Important radicals were labelled in pink. Note that no convinced signals of HOM dimers were observed in the 2nd-round experiments with $NO_x$.

**(a)**

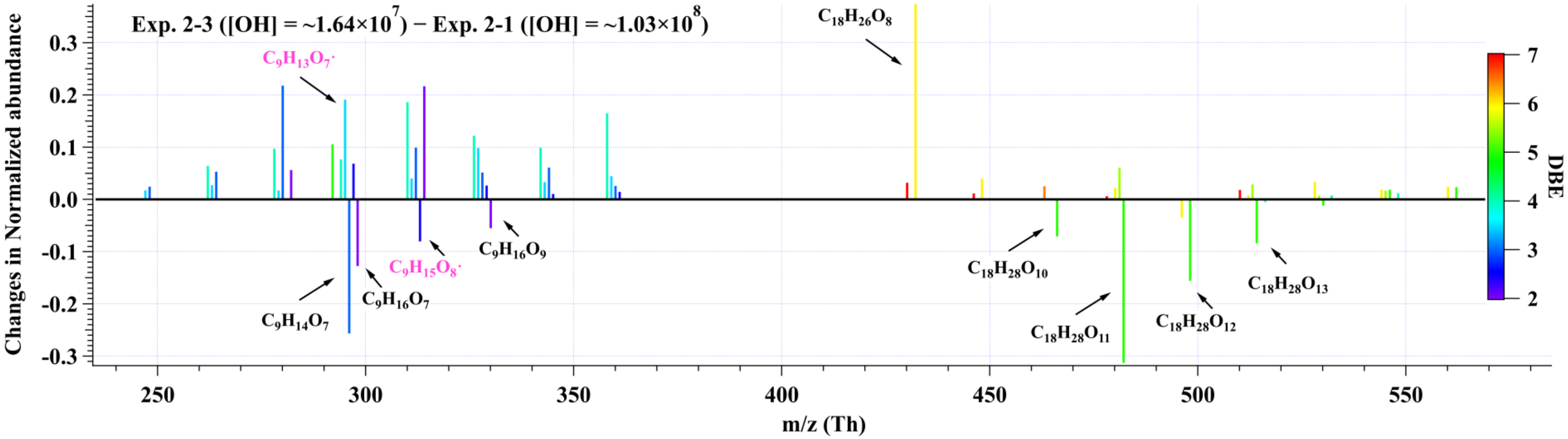

Exp. 2-3 ([OH] = ~1.64×10^7) − Exp. 2-1 ([OH] = ~1.03×10^8)
$C_{18}H_{26}O_8$
$C_9H_{13}O_7\cdot$
$C_9H_{15}O_8\cdot$
$C_9H_{16}O_9$
$C_9H_{14}O_7$
$C_9H_{16}O_7$
$C_{18}H_{28}O_{10}$
$C_{18}H_{28}O_{11}$
$C_{18}H_{28}O_{12}$
$C_{18}H_{28}O_{13}$
Changes in Normalized abundance
0.3
0.2
0.1
0.0
-0.1
-0.2
-0.3
250
300
350
400
450
500
550
m/z (Th)
DBE
7
6
5
4
3
2

**(b)**

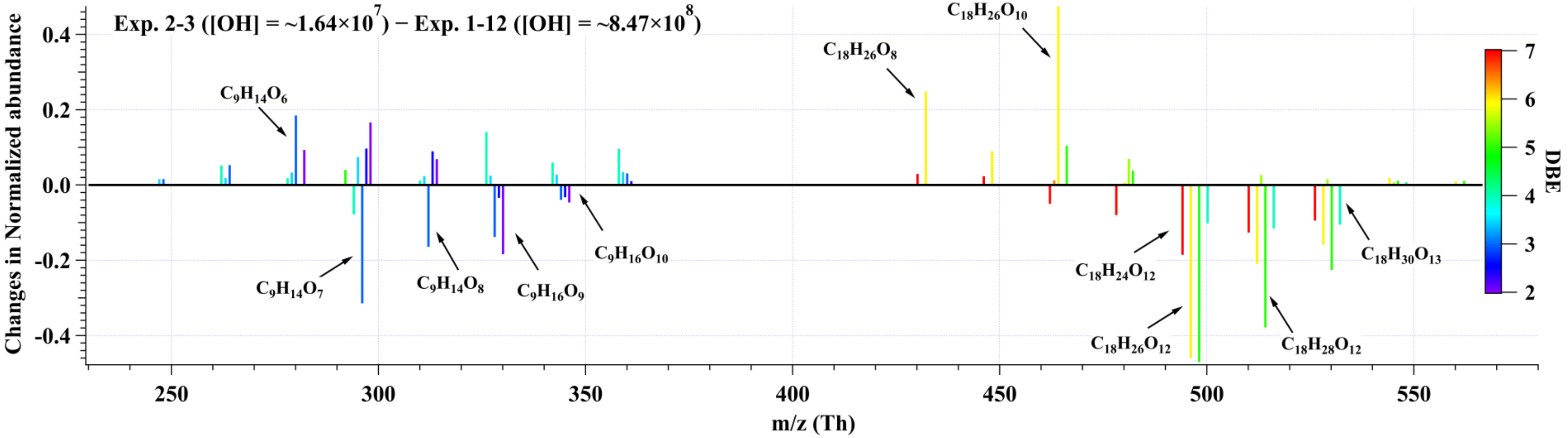

**Figure 6**. The changes in normalized abundance of C9 and C18 products observed by nitrate CI-TOF in (a) Exp.2-3 relative to Exp.2-1, and (b) Exp.2-3 relative to Exp.1-12. The reagent ion, $NO_3^-$, is omitted in the label. The normalized abundance was obtained by normalizing all the products to the most abundant one in each experiment, i.e., $C_{18}H_{26}O_{10}$ in Exp.2-1 and Exp.2-3, and $C_9H_{14}O_7$ in Exp.1-12.

## 4 Atmospheric Implications

This study highlights the influences of OH exposure on the distribution and evolution of 1,3,5-TMB-derived HOMs. Secondary OH reactions can influence HOMs' composition by directly reacting with the stabilized first-generation oxidation products, leading to enhanced formation of HOMs, if the stabilized, first-generation oxidation products could survive from condensation loss onto pre-existing particles. Observation of organonitrates generated in the NO experiments further confirmed the secondary OH oxidation. Due to the elevated abundance and the reduced volatility of HOMs, growth rates of newly formed nanoparticles in the presence of HOMs could be raised, especially in high-OH environments, which prevails in the summer noon. Substantially high concentrations of OH have been frequently observed in polluted environments during summer, e.g., megacities in China (Tan et al., 2019), and thus more active secondary OH reactions are expected compared to wintertime. As a plausible consequence, seasonal differences of HOMs and new particle formation (NPF) are resulted (Qiao et al., 2021; Yao et al., 2018; Guo et al., 2022). Furthermore, previous studies suggest that high concentrations of NO can suppress the formation of HOMs via the suppression of autoxidation (Pye et al., 2019), but the influences of such a suppression could have been overestimated, since secondary OH reactions can continue to oxidize the stabilized organonitrates. Our conclusions help to explain the existing gap between model prediction and ambient measurement on the HOMs concentrations (Qi et al., 2018), and to build a global HOMs simulation model.

*Data availability.* Data used in this work are available upon request from the corresponding authors.

*Supplement.* The supplement related to this article is available online.

*Author contributions.* LW and Yuwei Wang designed the experiments. Yuwei Wang conducted the laboratory experiments. Yuwei Wang analyzed the data. Yuwei Wang and LW wrote the paper. All co-authors discussed the results and commented on the manuscript.

*Competing interests.* The authors declare that they have no conflict of interest.

*Acknowledgments.* This work was financially supported by the National Natural Science Foundation of China (21925601, 22127811). The authors declare no competing interests.

Yuwei Wang would like to thank Andrew T. Lambe, Peng Zhe, and Jose Jimenez for helpful discussions on PAM experiments.

# References

Berndt, T., Mentler, B., Scholz, W., Fischer, L., Herrmann, H., Kulmala, M., and Hansel, A.: Accretion Product Formation from Ozonolysis and OH Radical Reaction of α-Pinene: Mechanistic Insight and the Influence of Isoprene and Ethylene, Environ. Sci. Technol., 52, 11069–11077, https://doi.org/10.1021/acs.est.8b02210, 2018a.

Berndt, T., Scholz, W., Mentler, B., Fischer, L., Herrmann, H., Kulmala, M., and Hansel, A.: Accretion Product Formation from Self- and Cross-Reactions of RO2 Radicals in the Atmosphere, Angew. Chemie - Int. Ed., 57, 3820–3824, https://doi.org/10.1002/anie.201710989, 2018b.

Bianchi, F., Kurtén, T., Riva, M., Mohr, C., Rissanen, M. P., Roldin, P., Berndt, T., Crounse, J. D., Wennberg, P. O., Mentel, T. F., Wildt, J., Junninen, H., Jokinen, T., Kulmala, M., Worsnop, D. R., Thornton, J. A., Donahue, N., Kjaergaard, H. G., and Ehn, M.: Highly Oxygenated Organic Molecules (HOM) from Gas-Phase Autoxidation Involving Peroxy Radicals: A Key Contributor to Atmospheric Aerosol, Chem. Rev., 119, 3472–3509, https://doi.org/10.1021/acs.chemrev.8b00395, 2019.

Cheng, X., Chen, Q., Li, Y. J., Zheng, Y., Liao, K., and Huang, G.: Highly Oxygenated Organic Molecules Produced by the Oxidation of Benzene and Toluene in a Wide Range of OH Exposure and NOx Conditions, Atmos. Chem. Phys., 1–23, https://doi.org/10.5194/acp-2021-201, 2021.

Crounse, J. D., Nielsen, L. B., Jørgensen, S., Kjaergaard, H. G., and Wennberg, P. O.: Autoxidation of organic compounds in the atmosphere, J. Phys. Chem. Lett., 4, 3513–3520, https://doi.org/10.1021/jz4019207, 2013.

Deng, C., Fu, Y., Dada, L., Yan, C., Cai, R., Yang, D., Zhou, Y., Yin, R., Lu, Y., Li, X., Qiao, X., Fan, X., Nie, W., Kontkanen, J., Kangasluoma, J., Chu, B., Ding, A., Kerminen, V. M., Paasonen, P., Worsnop, D. R., Bianchi, F., Liu, Y., Zheng, J., Wang, L., Kulmala, M., and Jiang, J.: Seasonal characteristics of new particle formation and growth in urban Beijing, Environ. Sci. Technol., 54, 8547–8557, https://doi.org/10.1021/acs.est.0c00808, 2020.

Ehn, M., Thornton, J. A., Kleist, E., Sipilä, M., Junninen, H., Pullinen, I., Springer, M., Rubach, F., Tillmann, R., Lee, B., Lopez-Hilfiker, F., Andres, S., Acir, I. H., Rissanen, M., Jokinen, T., Schobesberger, S., Kangasluoma, J., Kontkanen, J., Nieminen, T., Kurtén, T., Nielsen, L. B., Jørgensen, S., Kjaergaard, H. G., Canagaratna, M., Maso, M. D., Berndt, T., Petäjä, T., Wahner, A., Kerminen, V. M., Kulmala, M., Worsnop, D. R., Wildt, J., and Mentel, T. F.: A large source of low-volatility secondary organic aerosol, Nature, 506, 476–479, https://doi.org/10.1038/nature13032, 2014.

Eisele, F. L. and Tanner, D. J.: Measurement of the gas phase concentration of H 2 SO 4 and methane sulfonic acid and estimates of H 2 SO 4 production and loss in the atmosphere, J. Geophys. Res. Atmos., 98, 9001–9010, https://doi.org/10.1029/93JD00031, 1993.

Garmash, O., Rissanen, M. P., Pullinen, I., Schmitt, S., Kausiala, O., Tillmann, R., Zhao, D., Percival, C., Bannan, T. J., Priestley, M., Hallquist, Å. M., Kleist, E., Kiendler-Scharr, A., Hallquist, M., Berndt, T., McFiggans, G., Wildt, J., Mentel, T. F., and Ehn, M.: Multi-generation OH oxidation as a source for highly oxygenated organic molecules from aromatics, Atmos. Chem. Phys., 20, 515–537, https://doi.org/10.5194/acp-20-515-2020, 2020.

Guo, Y., Yan, C., Liu, Y., Qiao, X., Zheng, F., Zhang, Y., Zhou, Y., Li, C., Fan, X., Lin, Z., Feng, Z., Zhang, Y., Zheng, P., Tian, L., Nie, W., Wang, Z., Huang, D., Daellenbach, K. R., Yao, L., Dada, L., Bianchi, F., Jiang, J., Liu, Y., Kerminen, V. M., and Kulmala, M.: Seasonal variation in oxygenated organic molecules in urban Beijing and their contribution to secondary organic aerosol, Atmos. Chem. Phys., 22, 10077–10097, https://doi.org/10.5194/acp-22-10077-2022, 2022.

Heinritzi, M., Simon, M., Steiner, G., Wagner, A. C., Kürten, A., Hansel, A., and Curtius, J.: Characterization of the mass-dependent transmission efficiency of a CIMS, Atmos. Meas. Tech., 9, 1449–1460, https://doi.org/10.5194/amt-9-1449-2016, 2016.

Hyttinen, N., Kupiainen-Määttä, O., Rissanen, M. P., Muuronen, M., Ehn, M., and Kurtén, T.: Modeling the Charging of Highly Oxidized Cyclohexene Ozonolysis Products Using Nitrate-Based Chemical Ionization, J. Phys. Chem. A, 119, 6339–6345, https://doi.org/10.1021/acs.jpca.5b01818, 2015.

Iyer, S., Kumar, A., Savolainen, A., Barua, S., Daub, C., Pichelstorfer, L., Roldin, P., Garmash, O., Seal, P., Kurtén, T., and Rissanen, M.: Molecular rearrangement of bicyclic peroxy radicals is a key route to aerosol from aromatics, Nat. Commun., 14, 4984, https://doi.org/10.1038/s41467-023-40675-2, 2023.

Jacob, D. J.: Introduction to atmospheric chemistry, Princeton, 1999.

Jenkin, M. E., Saunders, S. M., Wagner, V., and Pilling, M. J.: Protocol for the development of the Master Chemical Mechanism, MCM v3 (Part B): tropospheric degradation of aromatic volatile organic compounds, Atmos. Chem. Phys., 3, 181–193, https://doi.org/10.5194/acp-3-181-2003, 2003.

Jenkin, M. E., Valorso, R., Aumont, B., Rickard, A. R., and Wallington, T. J.: Estimation of rate coefficients and branching ratios for gas-phase reactions of OH with aliphatic organic compounds for use in automated mechanism construction, 9297–9328 pp., https://doi.org/10.5194/acp-18-9297-2018, 2018a.

Jenkin, M. E., Valorso, R., Aumont, B., Rickard, A. R., and Wallington, T. J.: Estimation of rate coefficients and branching ratios for gas-phase reactions of OH with aromatic organic compounds for use in automated mechanism construction, Atmos. Chem. Phys., 18, 9329–9349, https://doi.org/10.5194/acp-18-9329-2018, 2018b.

Keller-Rudek, H., Moortgat, G. K., Sander, R., and Sörensen, R.: The MPI-Mainz UV/VIS spectral atlas of gaseous molecules of atmospheric interest, Earth Syst. Sci. Data, 5, 365–373, https://doi.org/10.5194/essd-5-365-2013, 2013.

Krechmer, J., Lopez-Hilfiker, F., Koss, A., Hutterli, M., Stoermer, C., Deming, B., Kimmel, J., Warneke, C., Holzinger, R., Jayne, J., Worsnop, D., Fuhrer, K., Gonin, M., and De Gouw, J.: Evaluation of a New Reagent-Ion Source and Focusing Ion− Molecule Reactor for Use in Proton-Transfer-Reaction Mass Spectrometry, Anal. Chem., 90, 12011–12018, https://doi.org/10.1021/acs.analchem.8b02641, 2018.

Lambe, A., Massoli, P., Zhang, X., Canagaratna, M., Nowak, J., Daube, C., Yan, C., Nie, W., Onasch, T., Jayne, J., Kolb, C., Davidovits, P., Worsnop, D., and Brune, W.: Controlled nitric oxide production via O(1D) + N2O reactions for use in oxidation flow reactor studies, Atmos. Meas. Tech., 10, 2283–2298, https://doi.org/10.5194/amt-10-2283-2017, 2017.

Lambe, A., Krechmer, J., Peng, Z., Casar, J., Carrasquillo, A., Raff, J., Jimenez, J., and Worsnop, D.: HO x and NO x production in oxidation flow reactors via photolysis of, 1–22, 2018.

Lambe, A. T., Ahern, A. T., Williams, L. R., Slowik, J. G., Wong, J. P. S., Abbatt, J. P. D., Brune, W. H., Ng, N. L., Wright, J. P., Croasdale, D. R., Worsnop, D. R., Davidovits, P., and Onasch, T. B.: Characterization of aerosol photooxidation flow reactors: heterogeneous oxidation, secondary organic aerosol formation and cloud condensation nuclei activity measurements, Atmos. Meas. Tech, 4, 445–461, https://doi.org/10.5194/amt-4-445-2011, 2011.

Lambe, A. T., Chhabra, P. S., Onasch, T. B., Brune, W. H., Hunter, J. F., Kroll, J. H., Cummings, M. J., Brogan, J. F., Parmar, Y., Worsnop, D. R., Kolb, C. E., and Davidovits, P.: Effect of oxidant concentration, exposure time, and seed particles on secondary organic aerosol chemical composition and yield, Atmos. Chem. Phys., 15, 3063–3075, https://doi.org/10.5194/acp-15-3063-2015, 2015.

Lehtipalo, K., Yan, C., Dada, L., Bianchi, F., Xiao, M., Wagner, R., Stolzenburg, D., Ahonen, L. R., Amorim, A., Baccarini, A., Bauer, P. S., Baumgartner, B., Bergen, A., Bernhammer, A. K., Breitenlechner, M., Brilke, S., Buchholz, A., Mazon, S. B., Chen, D., Chen, X., Dias, A., Dommen, J., Draper, D. C., Duplissy, J., Ehn, M., Finkenzeller, H., Fischer, L., Frege, C., Fuchs, C., Garmash, O., Gordon, H., Hakala, J., He, X., Heikkinen, L., Heinritzi, M., Helm, J. C., Hofbauer, V., Hoyle, C. R., Jokinen, T., Kangasluoma, J., Kerminen, V. M., Kim, C., Kirkby, J., Kontkanen, J., Kürten, A., Lawler, M. J., Mai, H., Mathot, S., Mauldin, R. L., Molteni, U., Nichman, L., Nie, W., Nieminen, T., Ojdanic, A., Onnela, A., Passananti, M., Petäjä, T., Piel, F., Pospisilova, V., Quéléver, L. L. J., Rissanen, M. P., Rose, C., Sarnela, N., Schallhart, S., Schuchmann, S., Sengupta, K., Simon, M., Sipilä, M., Tauber, C., Tomé, A., Tröstl, J., Väisänen, O., Vogel, A. L., Volkamer, R., Wagner, A. C., Wang, M., Weitz, L., Wimmer, D., Ye, P., Ylisirniö, A., Zha, Q., Carslaw, K. S., Curtius, J., Donahue, N. M., Flagan, R. C., Hansel, A., Riipinen, I., Virtanen, A., Winkler, P. M., Baltensperger, U., Kulmala, M., and Worsnop, D. R.: Multicomponent new particle formation from sulfuric acid, ammonia, and biogenic vapors, Sci. Adv., 4, 1–10, https://doi.org/10.1126/sciadv.aau5363, 2018.

Li, R., Palm, B. B., Ortega, A. M., Hlywiak, J., Hu, W., Peng, Z., Day, D. A., Knote, C., Brune, W. H., De Gouw, J. A., and Jimenez, J. L.: Modeling the radical chemistry in an oxidation flow reactor: Radical formation and recycling, sensitivities, and the OH exposure estimation equation, J. Phys. Chem. A, 119, 4418–4432, https://doi.org/10.1021/jp509534k, 2015.

Lu, K. D., Rohrer, F., Holland, F., Fuchs, H., Bohn, B., Brauers, T., Chang, C. C., Häseler, R., Hu, M., Kita, K., Kondo, Y., Li, X., Lou, S. R., Nehr, S., Shao, M., Zeng, L. M., Wahner, A., Zhang, Y. H., and Hofzumahaus, A.: Observation and modelling of OH and HO2 concentrations in the Pearl River Delta 2006: A missing OH source in a VOC rich atmosphere, Atmos. Chem. Phys., 12, 1541–1569, https://doi.org/10.5194/acp-12-1541-2012, 2012.

Ma, X., Tan, Z., Lu, K., Yang, X., Chen, X., Wang, H., Chen, S., Fang, X., Li, S., Li, X., Liu, J., Liu, Y., Lou, S., Qiu, W., Wang, H., Zeng, L., and Zhang, Y.: OH and HO2 radical chemistry at a suburban site during the EXPLORE-YRD campaign in 2018, Atmos. Chem. Phys., 22, 7005–7028, https://doi.org/10.5194/acp-22-7005-2022, 2022.

Mehra, A., Wang, Y., E. Krechmer, J., Lambe, A., Majluf, F., A. Morris, M., Priestley, M., J. Bannan, T., J. Bryant, D., L. Pereira, K., F. Hamilton, J., R. Rickard, A., J. Newland, M., Stark, H., Croteau, P., T. Jayne, J., R. Worsnop, D., R. Canagaratna, M., Wang, L., and Coe, H.: Evaluation of the chemical composition of gas- And particle-phase products of aromatic oxidation, Atmos. Chem. Phys., 20, 9783–9803, https://doi.org/10.5194/acp-20-9783-2020, 2020.

Mentel, T. F., Springer, M., Ehn, M., Kleist, E., Pullinen, I., Kurtén, T., Rissanen, M., Wahner, A., and Wildt, J.: Formation of highly oxidized multifunctional compounds: Autoxidation of peroxy radicals formed in the ozonolysis of alkenes - Deduced from structure-product relationships, Atmos. Chem. Phys., 15, 6745–6765, https://doi.org/10.5194/acp-15-6745-2015, 2015.

Mohr, C., Thornton, J. A., Heitto, A., Lopez-hil, F. D., Lutz, A., Riipinen, I., Hong, J., Donahue, N. M., Hallquist, M., Petäjä, T., Kulmala, M., and Yli-juuti, T.: Molecular identification of organic vapors driving atmospheric nanoparticle growth, Nat. Commun., 1–7, https://doi.org/10.1038/s41467-019-12473-2, 2019.

Molteni, U., Bianchi, F., Klein, F., Haddad, I. El, Frege, C., Rossi, M. J., Dommen, J., and Baltensperger, U.: Formation of highly oxygenated organic molecules from aromatic compounds, Atmos. Chem. Phys, 18, 1909–1921, https://doi.org/10.5194/acp-18-1909-2018, 2018.

Ng, N. L., Canagaratna, M. R., Zhang, Q., Jimenez, J. L., Tian, J., Ulbrich, I. M., Kroll, J. H., Docherty, K. S., Chhabra, P. S., Bahreini, R., Murphy, S. M., Seinfeld, J. H., Hildebrandt, L., Donahue, N. M., Decarlo, P. F., Lanz, V. A., Prévôt, A. S. H., Dinar, E., Rudich, Y., and Worsnop, D. R.: Organic aerosol components observed in Northern Hemispheric datasets from Aerosol Mass Spectrometry, Atmos. Chem. Phys., 10, 4625–4641, https://doi.org/10.5194/acp-10-4625-2010, 2010.

Orlando, J. J. and Tyndall, G. S.: Laboratory studies of organic peroxy radical chemistry: An overview with emphasis on recent issues of atmospheric significance, Chem. Soc. Rev., 41, 6294–6317, https://doi.org/10.1039/c2cs35166h, 2012.

Otkjær, R. V., Jakobsen, H. H., Tram, C. M., and Kjaergaard, H. G.: Calculated Hydrogen Shift Rate Constants in Substituted Alkyl Peroxy Radicals, J. Phys. Chem. A, 122, 8665–8673, https://doi.org/10.1021/acs.jpca.8b06223, 2018.

Peng, Z. and Jimenez, J. L.: Radical chemistry in oxidation flow reactors for atmospheric chemistry research, Chem. Soc. Rev., 49, 2570–2616, https://doi.org/10.1039/c9cs00766k, 2020.

Peng, Z., Day, D. A., Ortega, A. M., Palm, B. B., Hu, W., Stark, H., Li, R., Tsigaridis, K., Brune, W. H., and Jimenez, J. L.: Non-OH chemistry in oxidation flow reactors for the study of atmospheric chemistry systematically examined by modeling, Atmos. Chem. Phys., 16, 4283–4305, https://doi.org/10.5194/acp-16-4283-2016, 2016.

Pye, H. O. T., D'Ambro, E. L., Lee, B. H., Schobesberger, S., Takeuchi, M., Zhao, Y., Lopez-Hilfiker, F., Liu, J., Shilling, J. E., Xing, J., Mathur, R., Middlebrook, A. M., Liao, J., Welti, A., Graus, M., Warneke, C., de Gouw, J. A., Holloway, J. S., Ryerson, T. B., Pollack, I. B., and Thornton, J. A.: Anthropogenic enhancements to production of highly oxygenated molecules from autoxidation, Proc. Natl. Acad. Sci. U. S. A., 116, 6641–6646, https://doi.org/10.1073/pnas.1810774116, 2019.

Qi, X., Ding, A., Roldin, P., Xu, Z., Zhou, P., Sarnela, N., Nie, W., Huang, X., Rusanen, A., Ehn, M., Rissanen, M. P., Petäjä, T., Kulmala, M., and Boy, M.: Modelling studies of HOMs and their contributions to new particle formation and growth: comparison of boreal forest in Finland and a polluted environment in China, Atmos. Chem. Phys, 18, 11779–11791, https://doi.org/10.5194/acp-18-11779-2018, 2018.

Qiao, X., Yan, C., Li, X., Guo, Y., Yin, R., Deng, C., Li, C., Nie, W., Wang, M., Cai, R., Huang, D., Wang, Z., Yao, L., Worsnop, D. R., Bianchi, F., Liu, Y., Donahue, N. M., Kulmala, M., and Jiang, J.: Contribution of Atmospheric Oxygenated Organic Compounds to Particle Growth in an Urban Environment, Environ. Sci. Technol., https://doi.org/10.1021/acs.est.1c02095, 2021.

Qu, H., Wang, Y., Zhang, R., Liu, X., Huey, L. G., Sjostedt, S., Zeng, L., Lu, K., Wu, Y., Shao, M., Hu, M., Tan, Z., Fuchs, H., Broch, S., Wahner, A., Zhu, T., and Zhang, Y.: Chemical Production of Oxygenated Volatile Organic Compounds Strongly Enhances Boundary-Layer Oxidation Chemistry and Ozone Production, Environ. Sci. Technol., 55, 13718–13727, https://doi.org/10.1021/acs.est.1c04489, 2021.

Saunders, S. M., Jenkin, M. E., Derwent, R. G., and Pilling, M. J.: Protocol for the development of the Master Chemical Mechanism, MCM v3 (Part A): Tropospheric degradation of non-aromatic volatile organic compounds, Atmos. Chem. Phys., 3, 161–180, https://doi.org/10.5194/acp-3-161-2003, 2003.

Stolzenburg, D., Fischer, L., Vogel, A. L., Heinritzi, M., Schervish, M., Simon, M., Wagner, A. C., Dada, L., Ahonen, L. R., Amorim, A., Baccarini, A., Bauer, P. S., Baumgartner, B., Bergen, A., Bianchi, F., Breitenlechner, M., Brilke, S., Mazon, S. B., Chen, D., Dias, A., Draper, D. C., Duplissy, J., Haddad, I. El, Finkenzeller, H., Frege, C., Fuchs, C., Garmash, O., Gordon, H., He, X., Helm, J., Hofbauer, V., Hoyle, C. R., Kim, C., Kirkby, J., Kontkanen, J., Kürten, A., Lampilahti, J., Lawler, M., Lehtipalo, K., Leiminger, M., Mai, H., Mathot, S., Mentler, B., Molteni, U., Nie, W., Nieminen, T., Nowak, J. B., Ojdanic, A., Onnela, A., Passananti, M., Petäjä, T., Quéléver, L. L. J., Rissanen, M. P., Sarnela, N., Schallhart, S., Tauber, C., Tomé, A., Wagner, R., Wang, M., Weitz, L., Wimmer, D., Xiao, M., Yan, C., Ye, P., Zha, Q., Baltensperger, U., Curtius, J., Dommen, J., Flagan, R. C., Kulmala, M., Smith, J. N., Worsnop, D. R., Hansel, A., Donahue, N. M., and Winkler, P. M.: Rapid growth of organic aerosol nanoparticles over a wide tropospheric temperature range, Proc. Natl. Acad. Sci. U. S. A., 115, 9122–9127, https://doi.org/10.1073/pnas.1807604115, 2018.

Tan, Z., Fuchs, H., Lu, K., Hofzumahaus, A., Bohn, B., Broch, S., Dong, H., Gomm, S., Häseler, R., He, L., Holland, F., Li, X., Liu, Y., Lu, S., Rohrer, F., Shao, M., Wang, B., Wang, M., Wu, Y., Zeng, L., Zhang, Y., Wahner, A., and Zhang, Y.: Radical chemistry at a rural site (Wangdu) in the North China Plain: Observation and model calculations of OH, HO2 and RO2 radicals, Atmos. Chem. Phys., 17, 663–690, https://doi.org/10.5194/acp-17-663-2017, 2017.

Tan, Z., Rohrer, F., Lu, K., Ma, X., Bohn, B., Broch, S., Dong, H., Fuchs, H., Gkatzelis, G. I., Hofzumahaus, A., Holland, F., Li, X., Liu, Y., Liu, Y., Novelli, A., Shao, M., Wang, H., Wu, Y., Zeng, L., Hu, M., Kiendler-Scharr, A., Wahner, A., and Zhang, Y.: Wintertime photochemistry in Beijing: Observations of ROx radical concentrations in the North China

Plain during the BEST-ONE campaign, Atmos. Chem. Phys., https://doi.org/10.5194/acp-18-12391-2018, 2018.

Tan, Z., Lu, K., Jiang, M., Su, R., Wang, H., Lou, S., Fu, Q., Zhai, C., Tan, Q., Yue, D., Chen, D., Wang, Z., Xie, S., Zeng, L., and Zhang, Y.: Daytime atmospheric oxidation capacity in four Chinese megacities during the photochemically polluted season: A case study based on box model simulation, Atmos. Chem. Phys., 19, 3493–3513, https://doi.org/10.5194/acp-19-3493-2019, 2019.

Tröstl, J., Chuang, W. K., Gordon, H., Heinritzi, M., Yan, C., Molteni, U., Ahlm, L., Frege, C., Bianchi, F., Wagner, R., Simon, M., Lehtipalo, K., Williamson, C., Craven, J. S., Duplissy, J., Adamov, A., Almeida, J., Bernhammer, A. K., Breitenlechner, M., Brilke, S., Dias, A., Ehrhart, S., Flagan, R. C., Franchin, A., Fuchs, C., Guida, R., Gysel, M., Hansel, A., Hoyle, C. R., Jokinen, T., Junninen, H., Kangasluoma, J., Keskinen, H., Kim, J., Krapf, M., Kürten, A., Laaksonen, A., Lawler, M., Leiminger, M., Mathot, S., Möhler, O., Nieminen, T., Onnela, A., Petäjä, T., Piel, F. M., Miettinen, P., Rissanen, M. P., Rondo, L., Sarnela, N., Schobesberger, S., Sengupta, K., Sipilä, M., Smith, J. N., Steiner, G., Tomè, A., Virtanen, A., Wagner, A. C., Weingartner, E., Wimmer, D., Winkler, P. M., Ye, P., Carslaw, K. S., Curtius, J., Dommen, J., Kirkby, J., Kulmala, M., Riipinen, I., Worsnop, D. R., Donahue, N. M., and Baltensperger, U.: The role of low-volatility organic compounds in initial particle growth in the atmosphere, Nature, 533, 527–531, https://doi.org/10.1038/nature18271, 2016.

Tsiligiannis, E., Hammes, J., Salvador, C. M., Mentel, T. F., and Hallquist, M.: Effect of NOx on 1,3,5-trimethylbenzene (TMB) oxidation product distribution and particle formation, Atmos. Chem. Phys., 19, 15073–15086, https://doi.org/10.5194/acp-19-15073-2019, 2019.

Vereecken, L.: Reaction Mechanisms for the Atmospheric Oxidation of Monocyclic Aromatic Compounds, Adv. Atmos. Chem., 377–527, https://doi.org/10.1142/9789813271838_0006, 2019.

Wang, M., Chen, D., Xiao, M., Ye, Q., Stolzenburg, D., Hofbauer, V., Ye, P., Vogel, A. L., Mauldin, R. L., Amorim, A., Baccarini, A., Baumgartner, B., Brilke, S., Dada, L., Dias, A., Duplissy, J., Finkenzeller, H., Garmash, O., He, X. C., Hoyle, C. R., Kim, C., Kvashnin, A., Lehtipalo, K., Fischer, L., Molteni, U., Petäjä, T., Pospisilova, V., Quéléver, L. L. J., Rissanen, M., Simon, M., Tauber, C., Tomé, A., Wagner, A. C., Weitz, L., Volkamer, R., Winkler, P. M., Kirkby, J., Worsnop, D. R., Kulmala, M., Baltensperger, U., Dommen, J., El-Haddad, I., and Donahue, N. M.: Photo-oxidation of Aromatic Hydrocarbons Produces Low-Volatility Organic Compounds, Environ. Sci. Technol., 54, 7911–7921, https://doi.org/10.1021/acs.est.0c02100, 2020a.

Wang, S., Wu, R., Berndt, T., Ehn, M., and Wang, L.: Formation of Highly Oxidized Radicals and Multifunctional Products from the Atmospheric Oxidation of Alkylbenzenes, Environ. Sci. Technol., 51, 8442–8449, https://doi.org/10.1021/acs.est.7b02374, 2017.

Wang, W., Yuan, B., Peng, Y., Su, H., Cheng, Y., and Yang, S.: Direct observations indicate photodegradable oxygenated VOCs as larger contributors to radicals and ozone production in the atmosphere, Atmos. Chem. Phys., 1–28, 2022.

Wang, Y., Mehra, A., Krechmer, J. E., Yang, G., Hu, X., Lu, Y., Lambe, A., Canagaratna, M., Chen, J., Worsnop, D., Coe, H., and Wang, L.: Oxygenated products formed from OH-initiated reactions of trimethylbenzene: autoxidation and accretion, Atmos. Chem. Phys., 20, 9563–9579, https://doi.org/10.5194/acp-20-9563-2020, 2020b.

Whalley, L. K., Slater, E. J., Woodward-Massey, R., Ye, C., Lee, J. D., Squires, F., Hopkins, J. R., Dunmore, R. E., Shaw, M., Hamilton, J. F., Lewis, A. C., Mehra, A., Worrall, S. D., Bacak, A., Bannan, T. J., Coe, H., Percival, C. J., Ouyang, B., Jones, R. L., Crilley, L. R., Kramer, L. J., Bloss, W. J., Vu, T., Kotthaus, S., Grimmond, S., Sun, Y., Xu, W., Yue, S., Ren, L., Joe, W., Nicholas Hewitt, C., Wang, X., Fu, P., and Heard, D. E.: Evaluating the sensitivity of radical chemistry and ozone formation to ambient VOCs and NOxin Beijing, Atmos. Chem. Phys., 21, 2125–2147, https://doi.org/10.5194/acp-21-2125-2021, 2021.

Xu, L., Møller, K. H., Crounse, J. D., Kjaergaard, H. G., and Wennberg, P. O.: New insights into the radical chemistry and product distribution in the OH-initiated oxidation of benzene, Environ. Sci. Technol., 54, 13467–13477, https://doi.org/10.1021/acs.est.0c04780, 2020.

Yang, C., Yao, N., Xu, L., Chen, G., Wang, Y., Fan, X., Zhou, P., Clusius, P., Tham, Y. J., Lin, Z., Chen, Y., Li, M., Hong, Y., and Chen, J.: Molecular Composition of Anthropogenic Oxygenated Organic Molecules and Their Contribution to Organic Aerosol in a Coastal City, Environ. Sci. Technol., 57, 15956–15967, https://doi.org/10.1021/acs.est.3c03244, 2023.

Yao, L., Garmash, O., Bianchi, F., Zheng, J., Yan, C., Kontkanen, J., Junninen, H., Mazon, S. B., Ehn, M., Paasonen, P., Sipilä, M., Wang, M., Wang, X., Xiao, S., Chen, H., Lu, Y., Zhang, B., Wang, D., Fu, Q., Geng, F., Li, L., Wang, H., Qiao, L., Yang, X., Chen, J., Kerminen, V.-M., Petäjä, T., Worsnop, D. R., Kulmala, M., and Wang, L.: Atmospheric new particle formation from sulfuric acid and amines in a Chinese megacity, Science (80-. )., 361, 278–281, https://doi.org/10.1126/science.aao4839, 2018.

Yuan, B., Chen, W., Shao, M., Wang, M., Lu, S., Wang, B., Liu, Y., Chang, C. C., and Wang, B.: Measurements of ambient hydrocarbons and carbonyls in the Pearl River Delta (PRD), China, Atmos. Res., 116, 93–104, https://doi.org/10.1016/j.atmosres.2012.03.006, 2012.

Zaytsev, A., Koss, A. R., Breitenlechner, M., Krechmer, J. E., Nihill, K. J., Lim, C. Y., Rowe, J. C., Cox, J. L., Moss, J., Roscioli, J. R., Canagaratna, M. R., Worsnop, D. R., Kroll, J. H., and Keutsch, F. N.: Mechanistic study of the formation of ring-retaining and ring-opening products from the oxidation of aromatic compounds under urban atmospheric conditions, Atmos. Chem. Phys., 19, 15117–15129, https://doi.org/10.5194/acp-19-15117-2019, 2019.

Zhao, Y., Thornton, J. A., and Pye, H. O. T.: Quantitative constraints on autoxidation and dimer formation from direct probing of monoterpene-derived peroxy radical chemistry, Proc. Natl. Acad. Sci., 115, 12142–12147, https://doi.org/10.1073/pnas.1812147115, 2018.